Contrasting styles of peraluminous S-type and I-type granitic magmatism: Identification and implications for the accretionary history of the Chinese South Tianshan

Article *in* American Journal of Science · May 2022

DOI: 10.2475/02.2022.06

CITATIONS
0

READS
464

11 authors, including:

Zaili Tao
China University of Geosciences (Beijing)
8 PUBLICATIONS **19** CITATIONS
SEE PROFILE

Jiyuan Yin
Chinese Academy of Geological Sciences
36 PUBLICATIONS **934** CITATIONS
SEE PROFILE

Wenjiao Xiao
Chinese Academy of Sciences
805 PUBLICATIONS **39,048** CITATIONS
SEE PROFILE

Reimar Seltmann
Natural History Museum, London
309 PUBLICATIONS **8,018** CITATIONS
SEE PROFILE

[American Journal of Science, Vol. 322, February, 2022, P. 280–312, DOI 10.2475/02.2022.06]

CONTRASTING STYLES OF PERALUMINOUS S-TYPE AND I-TYPE GRANITIC MAGMATISM: IDENTIFICATION AND IMPLICATIONS FOR THE ACCRETIONARY HISTORY OF THE CHINESE SOUTH TIANSHAN

ZAILI TAO*,**, JIYUAN YIN*,***,†, WENJIAO XIAO§,§§, REIMAR SELTMANN§§§, WEN CHEN*, MIN SUN***, TAO WANG*, CHAO YUAN‡, STUART N. THOMSON‡‡, YUELONG CHEN**, and XIAOPING XIA‡

ABSTRACT. Peraluminous granitoids have aluminum saturation indices (A/CNK) higher than 1.0, which overlap to some extent between S- and I-type granitoids. However, their source and petrogenesis are still disputed. For example, whole-rock compositions alone are not always a valid way to discriminate the sources of peraluminous granitoids. To identify the geochemical affinities, source and petrogenesis of the peraluminous granitoids, we present new geochemical data, in situ zircon U-Pb ages and Hf-O isotopic data, and whole-rock Sr-Nd isotopic data for the peraluminous granitoids in the South Tianshan Orogen Belt (STOB), Northwesten China. Zircon U-Pb ages suggest that these peraluminous granitoids were emplaced in the latest Carboniferous (ca. 299 Ma). They contain the diagnostic mineral muscovite and have high $\delta^{18}O_{Zrn}$ values (>8.0 ‰) demonstrating a close affinity with S-type granitoids. Their low $\varepsilon Nd(t)$ values (−5.3 to −7.6), combined with variable zircon $\varepsilon Hf(t)$ values (−0.35 to −10.18), indicate that these S-type granitoids were likely derived from partial melting of metasedimentary rocks. In addition, inherited zircon cores from the S-type granitoids have variable $\delta^{18}O$ values (6.34–10.5 ‰) and zircon $\varepsilon Hf(t)$ values (−4.3 to −16.3), with age populations (ca. 400 to 500 Ma) similar to those of detrital zircons from late Carboniferous metasedimentary rocks in the region. These data show that the S-type granitoids were dominantly derived from late Carboniferous metasedimentary rocks rather than Precambrian crustal materials. The studied granitoids have a transitional composition between I- and S-type granitoids, which could be related to low compositional maturity of the late Carboniferous metasedimentary source. According to the spatial and temporal distribution and petrogenesis of the Carboniferous intrusive rocks in the STOB, we propose that a slab roll-back model can account for the generation of late Carboniferous S-type granitoids in the STOB.

Key words: Peraluminous granitoids, South Tianshan Orogen Belt, Metasedimentary rocks, Slab roll-back

introduction

A separation of S-type granitoids from I-type granitoids was proposed by White and Chappell (1977), based on studies of granitoids from the Lachlan Fold Belt (LFB) of south-east Australia. Generally, S-type granitoids are characteristically

*Key Laboratory of Deep-Earth Dynamics of Ministry of Natural Resources, Institute of Geology, Chinese Academy of Geological Sciences, Beijing 100037, China
**School of Earth Sciences and Resources, China University of Geosciences, Beijing, 100083, China
***Department of Earth Sciences, The University of Hong Kong, Pokflam Road, Hong Kong, China
§State Key Laboratory of Lithospheric Evolution, Institute of Geology and Geophysics, Chinese Academy of Sciences, Beijing, 100029, China
§§Xinjiang Research Center for Mineral Resources, Xinjiang Institute of Ecology and Geography, Chinese Academy of Sciences, Urumqi, 830011, China
§§§Centre for Russian and Central EurAsian Mineral Studies (CERCAMS), Department of Earth Sciences, Natural History Museum, London SW7 5BD, United Kindom
‡State Key Laboratory of Isotope Geochemistry, Guangzhou Institute of Geochemistry, Chinese Academy of Sciences, Guangzhou, 510640, China
‡‡Department of Geosciences, University of Arizona, 1040 E. 4th Street, Tucson, Arizona 85721, USA
†Corresponding author E-mail address: yinjiyuan1983@163.com (J. Yin)

strongly peraluminous (A/CNK=molar $Al_2O_3/(CaO+Na_2O+K_2O)$. 1.1) and contain aluminum-rich minerals (such as garnet, cordierite and muscovite). I-type granitoids are characteristically metaluminous to weakly peraluminous (A/CNK < 1.1) and contain amphibole. S-type granitoids are generally considered to be derived from the partial melting of metasedimentary rocks, whereas I-type granitoids are generated by the partial melting of metaigneous rocks (Chappell and White, 1974; McCulloch and Chappell, 1982). Consequently, when dealing with granitoid petrogenesis, discrimination of geochemical affinities (I-type or S-type) of granitoids is of foremost importance. In this regard, subsequent studies argued that the contrasting variation trends in P_2O_5 and A/CNK versus SiO_2 are very effective in distinguishing the two types of granitoid in the LFB (Chappell, 1999; Stevens and others, 2007). However, these criteria are not always valid when used to distinguish peraluminous granitoids elsewhere in the world. For example, the peraluminous granitoids from the Cape Granite Suite (CGS) in South Africa exhibit a negative correlation between P_2O_5 and SiO_2 (Gao and others, 2016), similar to those of I-type granitoids, but these peraluminous granitoids have been proven to be typical S-type granitoids (Stevens and others, 2007; Villaros and others, 2009). Therefore, if no characteristic minerals such as amphibole or cordierite/garnet are present, determining the source of peraluminous granitoids is not straightforward.

The development of in situ microanalytical techniques for the determination of isotopic compositions in accessory minerals has been proven to be effective for the study of granitoid petrogenesis and continental crust evolution (Valley and others, 2005; Kemp and others, 2007). Zircon is a common and robust accessory mineral in granitoids that preserves the isotopic composition of its parent magma at the time of crystallization (Valley and others, 2005). Zircon Hf isotopic compositions can distinguish the relative contribution of juvenile crust and ancient continental crust materials (Griffin and others, 2002; Kemp and others, 2007). Zircon oxygen isotopic compositions are useful in tracing the recycling of supracrustal rocks, because oxygen isotopes (expressed as $\delta^{18}O$) are sensitive to involvement of a supracrustal component that experienced either high- or low-temperature water-rock interaction (Valley and others, 2005). Zircon O isotopic compositions can thus provide crucial clues to test whether peraluminous granitoids were derived from metasedimentary rocks (S-type) or metaigneous rocks (I-type).

The Central Asian Orogenic Belt (CAOB; fig. 1A), is one of the largest accretionary orogens in the world (Şengör and others, 1993; Jahn and others, 2000; Kröner and others, 2008), and was formed by multiple accretion and collision processes as a result of successive closure of several ancient ocean basins (Jahn and others, 2000; Xiao and others, 2009). The South Tianshan Orogenic Belt (STOB) occupies the southwestern margin of the CAOB, which formed through the northward subduction of the south Tianshan Ocean (Gao and others, 2009; Xiao and others, 2013). Previous researchers have shown that late Carboniferous to early Permian granitoids were widespread in the STOB (Konopelko and others, 2007; Zhu and others, 2008a; Ma and others, 2010; Seltmann and others, 2011). These granitoids are weakly peraluminous (A/CNK< 1.1; Zhu and others, 2008a; Ma and others, 2010; Huang and others, 2012), consistent with the geochemical features of I-type granitoids (Chappell and White, 2001). In contrast, they are characterized by negative $\varepsilon Nd(t)$ values and high K_2O/Na_2O ratios (. 1) (Konopelko and others, 2007, 2009; Ma and others, 2010; Huang and others, 2012) resembling S-type granitoids (Gao and others, 2014; Zhao and others, 2015). Thus, whether they can be ascribed as S-type or I-type is uncertain. In addition, the late Carboniferous tectonic setting is still a matter of debate in the STOB, with competing hypotheses including an intra-continental rift or mantle plume model (Zhang and Zuo, 2013; Han and Zhao, 2018; Han and others, 2019), a post-collisional

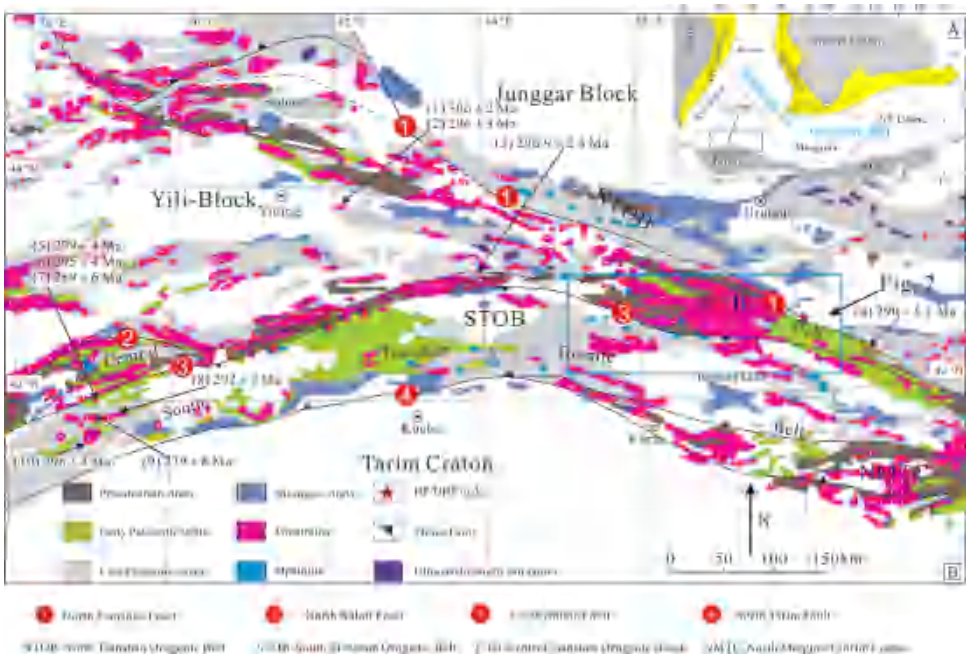

Fig. 1. (A) Simplified tectonic map of the CAOB (after Jahn and others, 2000), and (B) geological map of the Tianshan Orogenic Belt (modified from Gao and others, 2011). Data sources for the ages of granitic intrusions: (1) and (2) (Li and others, 2015); (3) (Xu and others, 2013) (4) (Dong and others, 2011) (5), (6) and (7) (Seltmann and others, 2011); (8), (9) and (10) (Konopelko and others, 2007).

environment (Gao and others, 2009; Long and others, 2011; Huang and others, 2011, 2012), or arc-related setting (Zhang and others, 2007; Xiao and others, 2013). Therefore, to overcome this controversy requires sophisticated ways to decipher distinct features of their petrogenesis and geodynamic environment.

In this contribution, we present new whole-rock major and trace element geochemistry, and Sr-Nd isotopic data, as well as zircon U-Pb, Hf-O isotopic data and zircon trace element compositions for the granitoids in the STOB, NW China. These data serve to clearly identify the rock types of these granitoids and provide better constraints on their magmatic source and petrogenesis. These findings also have significant implications for resolving the debate on the tectonic evolution of the STOB during the late Carboniferous.

geological setting and sampling

The Tianshan Orogenic Belt is situated in the southern part of the CAOB (fig. 1B; Windley and others, 2007; Xiao and others, 2008, 2009; Dong and others, 2011; Han and others, 2011). It extends west-east along the southwestern part of the CAOB from Uzbekistan, Tajikistan, Kyrgyzstan, and Kazakhstan to northwestern China (Şengör and others, 1993). The Chinese Tianshan Orogenic Belt is divided into two segments; the eastern Tianshan and the western Tianshan along 88°E (Li and others, 2006; Gao and others, 2009). From north to south, the western Tianshan is tectonically subdivided into the Northern Tianshan Orogenic Belt (NTOB), Yili-Central Tianshan Terrane (CTB) and South Tianshan Orogenic Belt (STOB) (Allen and others, 1993; Xiao and others, 2009), separated by the Northern Tianshan suture and Northern Tarim suture, respectively.

The STOB can be divided into western and eastern segment. The Chinese part of the STOB is mostly located in the eastern segment of the Talas-Fergana diagonal dextral strike-slip fault (Windley and others, 2007). The formation of the STOB was related to the northward subduction and closure of the south Tianshan Ocean and subsequent collision of the Tarim Craton to the south and the Yili-central Tianshan block to the north. The main body of the STOB is composed of imbricated Late Ordovician limestones, Silurian clastic sedimentary rocks, Devonian limestones, Carboniferous clastic rocks and volcanic interlayers (Xiao and others, 2013). Precambrian basement rocks in the STOB have not yet been clearly recognized (Han and others, 2016a). Moreover, subduction and/or collision related high-pressure/low-temperature (HP/LT) metamorphic rocks, ophiolitic mélanges or slices, mafic-ultramafic rocks, island arc assemblages and granitoids are also well preserved (Gao and others, 2009, 2011; Dong and others, 2011; Long and others, 2011). The HP-LT terranes are mainly composed of blueschist-, eclogite- and greenschist-facies metasedimentary rocks and some mafic meta-volcanic rocks with N-MORB, E-MORB and OIB affinities (Gao and others, 2009). Most HP-LT rocks have peak metamorphic ages varying from 320 to 310 Ma (Su and others, 2010; Li and others, 2011). Moreover, zircons from eclogites yield SHRIMP U-Pb ages of 226 to 233 Ma, which were interpreted to represent the timing of peak metamorphic conditions (Zhang and others, 2007). There are four ophiolite mélanges in the Chinese part of the STOB, from west to east, the Baleigong, Heiyingshan, Kulehu, and Kumux. These ophiolitic mélange units consist of serpentinized peridotites, diabase-gabbros, basalts, cherts, with metagreywackes and marls (Han and others, 2011), with zircon U-Pb age of 450 to 382 Ma (Wang and others, 2007; Wang and others, 2011; Zhu and others, 2008b). Paleozoic magmatism occurred predominantly in two periods: the late Silurian to Middle Devonian, and late Carboniferous to early Permian (Jiang and others, 1999; Konopelko and others, 2007, 2009; Ma and others, 2010; Huang and others, 2012). The former mainly consists of granodiorites, quartz monzonites and diorites (Long and others, 2011; Huang and others, 2015). The latter is predominantly composed of syenites, nepheline syenites, aegirine syenites, two-mica peraluminous leucogranitoids and A-type rapakivi granitoids (Jiang and others, 1999; Konopelko and others, 2007; Huang and others, 2012, 2015).

We collected 12 granitic samples including biotite granitoids and muscovite-bearing granitoids in the Hejing region of the STOB (figs. 2 and 3). The sampling locations are labeled in figure 2 and summarized in table 1. Muscovite-bearing granitoids include two-mica monzogranite (CT1604) and tonalite (CT1605). The two-mica monzogranites have medium-coarse grained textures, and are composed of plagioclase (35 vol.%), K-feldspar (35 vol.%), quartz (25 vol.%), biotite and muscovite (5 vol.%), with minor accessory minerals (apatite, and zircon) (figs. 4A and B). The tonalites are composed of plagioclase (50–60 vol.%), K-feldspar (10 vol.%), quartz (25 vol.%), biotite and muscovite (5–10 vol.%), with minor apatite, and zircon (figs. 4C and D). Biotite granitoids include monzogranite (CT1602) and quartz monzonite (CT1606). The monzogranites exhibit medium-grained granitic texture, and consist of plagioclase (35 vol.%), K-feldspar (35 vol.%), quartz (20%) and biotite (10%). The quartz monzonites are characterized by medium-grained textures, and mainly contain plagioclase (45 vol.%), K-feldspar (25 vol.%), quartz (20 vol.%) and biotite (10 vol.%), with minor apatite and zircon (figs. 4E and F).

analytical methods

U-Pb Zircon Geochronology

Zircon grains were separated using conventional standard density and magnetic separation, followed by hand-picking. Representative grains, together with the zircon

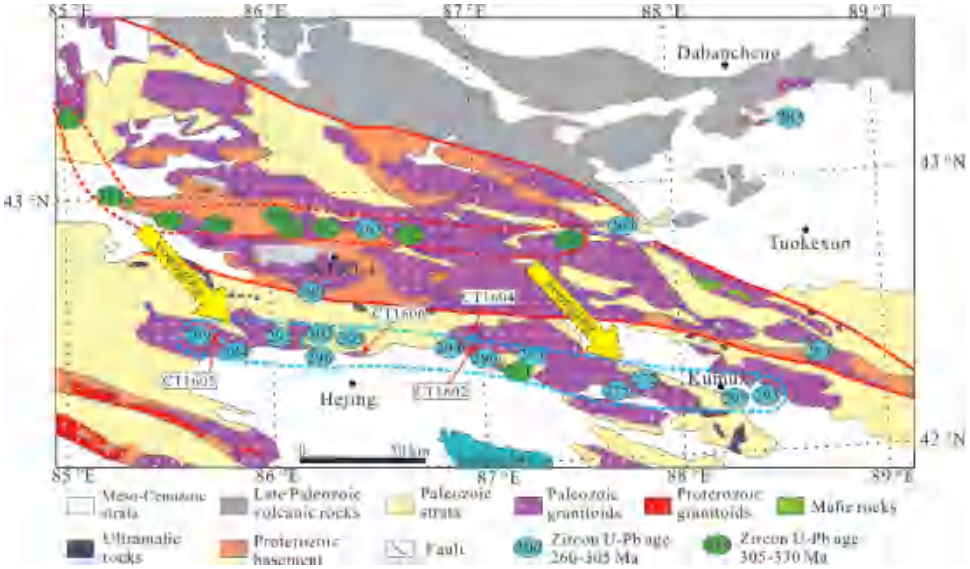

Fig. 2. Simplified geological map of the Hejing region in the STOB (modified after Ma and others, 2015), showing spatial and temporal distribution of the late Carboniferous-early Permian magmatic rocks in the CTB and STOB. Age data sources: Zhu and others (2008a), Tang and others (2012), Tian and others (2014), Ma and others (2015), Yang and others (2016), Yin and others (2015), Wang and others (2018), Chen and others (2019), Tao and others (2019), Reziwanguli and others (2019), Huang and others (2015, 2020).

standards, were mounted in epoxy and polished. All zircon grains were photographed in transmitted and reflected light as well as cathodoluminescence (CL) to study their internal structures. The LA-ICP-MS zircon U-Pb isotopic compositions for each sample were determined using an Agilent 7500a ICP-MS with an attached 193 nm excimer ArF laser-ablation system (GeoLas Plus) at the Institute of Geology and Geophysics, Chinese Academy of Sciences (IGG-CAS). The detailed experimental methods were described by Xie and others (2008). Analyses were acquired at a beam diameter of 32 lm, an 8 Hz repetition rate, and an energy of 10–20 J/cm2. Every 10 unknown analyses were followed by measurements of two zircon 91500, one GJ-1 and one NIST SRM 610 standards. Raw data were processed using GLITTER 4.0 program (Macquarie University). The zircons 91500 and GJ-1 were used as an external standard and internal standard, respectively. Trace element compositions of zircon were calibrated against NIST610 combined with internal standardization Si, and common Pb was corrected according to the method proposed by Andersen (2002). Analyses of the zircon standard GJ-1 as an unknown yielded a weighted mean $^{206}Pb/^{238}U$ age of 60464 Ma (1.2, n=9), which is in good agreement with the recommended value (Jackson and others, 2004). Isoplot (version 4.5) was used to draw U-Pb age harmonic plots and relative probability histograms (Ludwig, 2003). The LA-ICP-MS zircon U-Pb isotopic data are presented in table 2.

Major and Trace Elements

For geochemical analyses, after cleaning, crushing and homogenization, representative whole-rock samples were powdered to ; 200-mesh size. Major element compositions were analyzed on fused glass beads using a Rigaku RIX 2000 X-ray fluorescence spectrometer at the State Key Laboratory of Isotope Geochemistry, the

Fig. 3. Field and hand specimen photographs of the late Carboniferous granitic rocks from the Hejing region of the STOB.

Guangzhou Institute of Geochemistry, Chinese Academy of Sciences (GIG-CAS). Details of procedures are described by Yuan and others (2010). Trace elements, including REE, were determined using an ELAN DRC-e ICP-MS at the State Key Laboratory of Ore Deposit Geochemistry, Institute of Geochemistry, Chinese Academy of Sciences, following procedures described by Liang and others (2000).

TABLE 1

Summary of sample localities, zircon U–Pb ages and isotopic compositions of granitoid rocks in the South Tianshan

Sample	Ages	Lithology	GPS	$(^{87}Sr/^{86}Sr)_i$	$\varepsilon Nd_{(t)}$	$\varepsilon Hf_{(t)}$	$\delta^{18}O$
CT1602*	295.8±1.7 Ma	Biotite granitoids	42°28'34"; 86°55'19"	0.7092 ~ 0.7142	-5.3 ~ +2.0	-6.18 ~ +6.48	8.87 ~ 10.45 ‰
CT1604		Muscovite-bearing granitoids	42°29'19"; 86°55'15"	0.7133 ~ 0.7188	-5.8 ~ -5.5		
CT1605	298.5±2.0 Ma	Muscovite-bearing granitoids	42°27'58"; 85°43'30"	0.7086 ~ 0.7092	-7.6 ~ -6.9	-10.18 ~ -0.35	
CT1606	298.9±2.9 Ma	Biotite granitoids	42°25'18"; 86°27'32"	0.7080 ~ 0.7081	-5.4 ~ -5.8	-8.01 ~ -2.85	10.54~ 11.74 ‰

* The data are from Tao and others (2019).

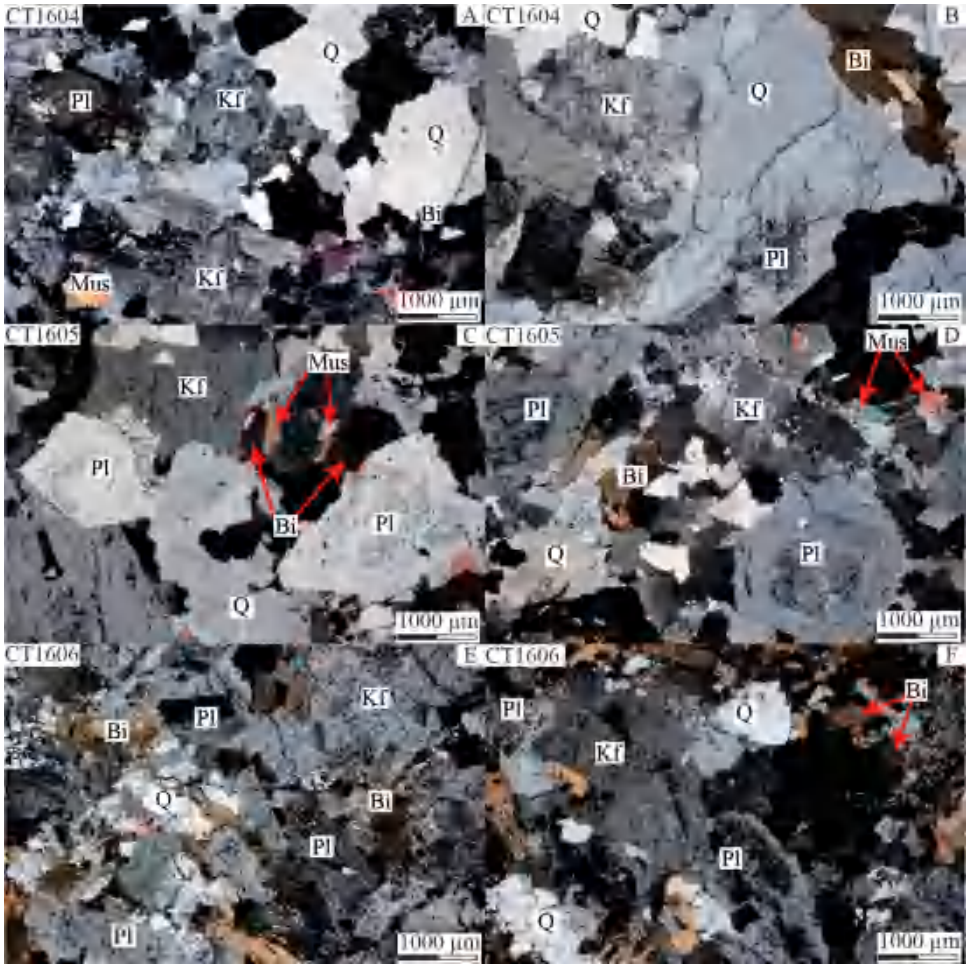

Fig. 4. Representative thin section photomicrographs of the late Carboniferous granitic rocks in the STOB. Pl = plagioclase, Kf = K feldspar, Bi = biotite, Q = quartz, Mus = muscovite, Cross-polarized light.

Sr-Nd Isotope Analyses

Sr-Nd isotopic compositions were performed using a Micromass Isoprobe multi-collector ICP-MS at the State Key Laboratory of Isotope Geochemistry, the Guangzhou Institute of Geochemistry, Chinese Academy of Sciences (GIG-CAS). Sr and Nd were separated using cation exchange columns, and Nd fractions were further separated by HDEHP-coated Kef columns. Detailed analytical procedures were described by Wei and others (2002) and Liang and others (2002). Measured $^{86}Sr/^{88}Sr$ and $^{143}Nd/^{144}Nd$ ratios were normalized to $^{86}Sr/^{88}Sr = 0.1194$ and $^{143}Nd/^{144}Nd = 0.7219$, respectively. External precisions during the period of measurement for Sr and Nd isotopic compositions were 6 0.000010 (n = 18), and 6 0.000011 (n = 18), respectively. The $^{87}Sr/^{86}Sr$ ratio for the NBS987 standard was 0.710274 6 18 (n = 11, 2r) and $^{143}Nd/^{144}Nd$ for JNdi-1 standard 0.512093 6 11 (n = 11, 2r).

TABLE 2

LA-ICP-MS zircon U-Pb ages of granitoid rocks in the South Tianshan

Analysis spot	Th(ppm)	U(ppm)	Th/U	$^{207}Pb/^{206}Pb$	1σ	$^{207}Pb/^{235}U$	1σ	$^{206}Pb/^{238}U$	1σ	$^{207}Pb/^{235}U$	1σ	$^{206}Pb/^{238}U$	1σ
Biotite granitoid (CT1602)													
CT1602@17	95	513	0.19	0.1035	0.0009	3.05	0.083	0.2141	0.0054	1415	21	1249	29
CT1602@18	71	197	0.36	0.0911	0.0008	3.27	0.038	0.2602	0.0027	1473	9.1	1490	14
CT1602@19	148	205	0.72	0.0532	0.0012	0.3803	0.0084	0.0525	0.0007	327	6.2	330	4.1
CT1602@20	1240	562	2.21	0.053	0.0008	0.3539	0.0057	0.0486	0.0005	308	4.3	306	3.2
CT1602@21	520	439	1.18	0.0536	0.0007	0.3605	0.0062	0.0492	0.0005	312	4.6	310	2.9
CT1602@22	242	646	0.37	0.0557	0.0007	0.5514	0.0085	0.0723	0.0011	446	5.6	450	6.4
CT1602@23	394	401	0.98	0.0547	0.0012	0.3551	0.0084	0.0474	0.0006	308	6.3	298	3.4
CT1602@24	256	376	0.68	0.0549	0.0015	0.382	0.011	0.0505	0.0005	328	8.3	318	2.8
CT1602@27	148	269	0.55	0.0521	0.0011	0.3931	0.0087	0.0552	0.0006	336	6.3	346	3.6
CT1602@32	457	791	0.58	0.0782	0.0022	0.784	0.056	0.0713	0.0032	578	30	443	19
Muscovite-bearing granitoid (CT1605)													
CT1605@1	238	569	0.42	0.0525	0.0028	0.3463	0.0182	0.0478	0.0006	302	14	301	4
CT1605@2	734	1666	0.44	0.0543	0.0013	0.3545	0.0086	0.0474	0.0005	308	6	298	3
CT1605@3	53	1091	0.05	0.052	0.0017	0.3414	0.0107	0.0476	0.0005	298	8	300	3
CT1605@4	99	257	0.38	0.0518	0.0062	0.3406	0.0402	0.0477	0.0009	298	30	300	6
CT1605@5	252	412	0.61	0.0529	0.0042	0.3472	0.0275	0.0476	0.0008	303	21	300	5
CT1605@6	246	1334	0.18	0.0532	0.0019	0.3485	0.012	0.0476	0.0006	304	9	299	4
CT1605@7	152	269	0.56	0.0526	0.0064	0.3427	0.0412	0.0473	0.001	299	31	298	6
CT1605@8	157	598	0.26	0.0521	0.0034	0.3433	0.0223	0.0478	0.0007	300	17	301	4
CT1605@9	307	450	0.68	0.0557	0.0022	0.5313	0.0212	0.0692	0.0009	433	14	431	5
CT1605@10	280	398	0.7	0.0593	0.0046	0.3858	0.0297	0.0472	0.0008	331	22	297	5
CT1605@11	7	742	0.01	0.0541	0.003	0.3545	0.0195	0.0476	0.0007	308	15	300	4
CT1605@12	438	520	0.84	0.0568	0.0027	0.5266	0.025	0.0672	0.0008	430	17	420	5
CT1605@13	275	1146	0.24	0.0522	0.0037	0.3482	0.0245	0.0484	0.0009	303	18	305	5
CT1605@14	253	1080	0.23	0.0552	0.0028	0.3613	0.0182	0.0475	0.0007	313	14	299	4
CT1605@15	181	305	0.59	0.0629	0.0075	0.4119	0.0484	0.0475	0.0012	350	35	299	8
CT1605@16	94	123	0.77	0.0655	0.0142	0.4212	0.0902	0.0467	0.0018	357	64	294	11

TABLE 2
(continued)

Analysis spot	Th(ppm)	U(ppm)	Th/U	$^{207}Pb/^{206}Pb$	1σ	$^{207}Pb/^{235}U$	1σ	$^{206}Pb/^{238}U$	1σ	$^{207}Pb/^{235}U$	1σ	$^{206}Pb/^{238}U$	1σ
Muscovite-bearing granitoid (CT1605)													
CT1605@17	86	108	0.79	0.0652	0.0213	0.4162	0.1344	0.0463	0.0025	353	96	292	16
CT1605@18	107	127	0.84	0.0631	0.0163	0.4014	0.1025	0.0461	0.0018	343	74	291	11
CT1605@19	144	545	0.26	0.0545	0.0043	0.3462	0.0267	0.0461	0.0006	302	20	290	4
CT1605@20	556	2288	0.24	0.0537	0.0026	0.3491	0.0162	0.0471	0.0005	304	12	297	3
CT1605@21	107	360	0.3	0.0719	0.0033	0.8622	0.0402	0.0871	0.0012	631	22	538	7
CT1605@22	257	314	0.82	0.0563	0.0066	0.366	0.0426	0.0472	0.001	317	32	297	6
CT1605@23	221	388	0.57	0.066	0.0054	0.4289	0.0347	0.0472	0.001	362	25	297	6
Biotite granitoid (CT1606)													
CT1606@1	165	213	0.78	0.0537	0.0078	0.3529	0.0508	0.0478	0.0012	307	38	301	8
CT1606@2	514	736	0.7	0.0461	0.0037	0.3012	0.0235	0.0474	0.0007	267	18	299	4
CT1606@3	377	382	0.99	0.0562	0.0046	0.3645	0.0294	0.0472	0.0009	316	22	297	5
CT1606@4	250	298	0.84	0.0522	0.0059	0.3406	0.0381	0.0474	0.0009	298	29	299	6
CT1606@5	199	282	0.71	0.0527	0.0055	0.3428	0.0356	0.0473	0.0009	299	27	298	6
CT1606@6	246	288	0.85	0.0524	0.0056	0.3497	0.037	0.0485	0.0009	304	28	305	6
CT1606@7	210	277	0.76	0.0615	0.006	0.3971	0.0385	0.0469	0.001	340	28	295	6
CT1606@8	166	224	0.74	0.0546	0.0061	0.354	0.0395	0.0471	0.0009	308	30	297	6
CT1606@9	353	531	0.67	0.0523	0.0034	0.3518	0.0228	0.0488	0.0007	306	17	307	4
CT1606@10	129	140	0.92	0.0342	0.0125	0.2326	0.0845	0.0493	0.0016	212	70	310	10
CT1606@11	233	334	0.7	0.0533	0.005	0.3618	0.0334	0.0493	0.0009	314	25	310	5
CT1606@12	253	303	0.83	0.0541	0.005	0.3556	0.0324	0.0477	0.0008	309	24	300	5
CT1606@13	247	240	1.03	0.0525	0.0076	0.3542	0.0507	0.0489	0.0012	308	38	308	7
CT1606@14	293	597	0.49	0.0519	0.0031	0.3491	0.0209	0.0488	0.0007	304	16	307	4
CT1606@15	273	313	0.87	0.0581	0.0052	0.3759	0.0335	0.0469	0.0009	324	25	296	5
CT1606@16	188	277	0.68	0.048	0.0068	0.3258	0.046	0.0492	0.0011	286	35	309	7
CT1606@17	346	380	0.91	0.047	0.0043	0.3172	0.0292	0.049	0.0008	280	22	308	5
CT1606@18	210	285	0.74	0.0492	0.0069	0.3304	0.0456	0.0486	0.0013	290	35	306	8
CT1606@19	172	270	0.64	0.052	0.0071	0.3501	0.0472	0.0487	0.0011	305	36	307	7

TABLE 2
(continued)

Analysis spot	Th(ppm)	U(ppm)	Th/U	$^{207}Pb/^{206}Pb$	1σ	$^{207}Pb/^{235}U$	1σ	$^{206}Pb/^{238}U$	1σ	$^{207}Pb/^{235}U$	1σ	$^{206}Pb/^{238}U$	1σ
Biotite granitoid (CT1606)													
CT1606@20	400	408	0.98	0.0507	0.0044	0.3341	0.0286	0.0477	0.0008	293	22	301	5
CT1606@21	446	479	0.93	0.0523	0.0047	0.3446	0.0309	0.0478	0.0009	301	23	301	6
CT1606@22	383	675	0.57	0.0521	0.0033	0.342	0.0218	0.0476	0.0007	299	17	300	4
CT1606@23	314	466	0.67	0.0521	0.0052	0.3486	0.0346	0.0485	0.001	304	26	305	6
CT1606@24	198	249	0.79	0.0531	0.0066	0.3458	0.0425	0.0471	0.0011	302	32	297	7
CT1606@25	307	345	0.89	0.0525	0.006	0.3593	0.0411	0.0496	0.0011	312	31	312	7
CT1606@26	108	133	0.81	0.0543	0.0018	0.342	0.011	0.0469	0.0011	301	9.6	295	7
CT1606@27	159	147	1.08	0.0524	0.0014	0.3294	0.0093	0.0466	0.0009	289	7.1	293	5.3
CT1606@30	206	175	1.18	0.0526	0.0012	0.3202	0.0079	0.0445	0.0008	282	6.1	281	4.7
CT1606@31	265	386	0.69	0.0531	0.0009	0.3401	0.0086	0.0481	0.0011	297	6.5	303	6.6
CT1606@32	145	151	0.96	0.0513	0.0011	0.3157	0.0077	0.0454	0.0007	278	5.9	286	4.4
CT1606@33	193	206	0.94	0.0517	0.0011	0.322	0.0088	0.0457	0.0009	283	6.8	288	5.4
CT1606@34	145	192	0.75	0.0525	0.0013	0.3503	0.0086	0.0494	0.0007	305	6.4	311	4.6
CT1606@36	143	222	0.65	0.0616	0.001	0.69	0.015	0.0823	0.0014	532	8.8	510	8
CT1606@38	189	181	1.05	0.0535	0.0015	0.332	0.0082	0.0453	0.0006	291	6.3	286	3.6
CT1606@40	213	229	0.93	0.0555	0.0012	0.3457	0.0081	0.0462	0.0006	301	6.1	291	3.7
CT1606@41	138	218	0.63	0.0741	0.0017	1.104	0.04	0.1091	0.0019	751	19	667	11

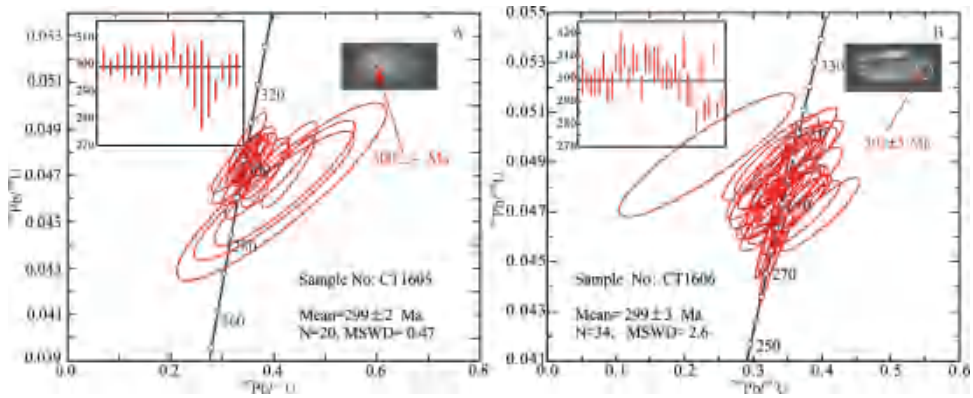

Fig. 5. Concordia diagrams with representative zircon CL images for LA-ICP-MS zircon analyses of studied late Carboniferous granitoids. (A) sample CT1605 from Muscovite-bearing granitoid, (B) sample CT1605 from Biotite granitoid..

Zircon Lu-Hf Isotopes

Lu-Hf isotope analyses were performed using a Nu Plasma HR MC-ICP-MS (Nu Instruments), coupled to a 193 nm excimer laser ablation system (Resolution M-50, Resonetics LLC), installed in the Institute of Geology and Geophysics, Chinese Academy of Sciences (IGG-CAS). Lu-Hf isotopic analyses were conducted on the same spots that were previously analyzed for U-Pb isotopes. Depending on the zircon size, a spot size of 60 lm or 40 lm was used for analysis, with a laser repetition rate of 6 Hz. Details on the instrumental conditions and data acquisition are given in Xie and others (2008). The measured $^{176}Hf/^{177}Hf$ ratios were normalized to $^{179}Hf/^{177}Hf = 0.7325$, using an exponential correction for mass bias. During analysis, the $^{176}Hf/^{177}Hf$ and $^{176}Lu/^{177}Hf$ ratios of the standard zircon (91500) were 0.282294 6 15 (20n, n = 20) and 0.00031, respectively, which is in good agreement with the low peaks of $^{176}Hf/^{177}Hf$ ratios of 0.282284 6 22 measured by Griffin and others (2006).

Zircon Oxygen Isotopes

Zircon oxygen isotope analyses was measured using the Cameca IMS-1280 HR ion microprobe at the GIG-CAS, Beijing. The detailed experimental methods are described by Li and others (2010a). The measured oxygen isotopic values were corrected for instrumental mass fractionation (IMF) using the standard Penglai zircon $d^{18}O_{VSMOW} = 5.3$ 6 0.10 % (2r) and Qinghu standards 5.4 6 0.2 % (2r) Li and others (2010b). The internal precision of a single analysis generally was better than 0.2 % (1r standard error) for the $^{18}O/^{16}O$ ratio, and using the standard Penglai zircon as an external standard to correct data, is 0.50 % (2SD, n = 68). Detailed analytical procedures are provided by Li and others (2010a).

results

Zircon U-Pb Geochronology

The zircon U-Pb isotopic data are given in table 2. The biotite granitoids and muscovite-bearing granitoids were selected for zircon U-Pb dating. Zircons in these samples have crystal lengths of ; 100 to 300 lm with length:width ratios from 1:1 to 3:1. A few zircon grains show clear core-rim structure in cathodoluminescence (CL) images (fig. 6B). LA-ICP-MS in situ U-Pb dating was performed on the zircon rims and

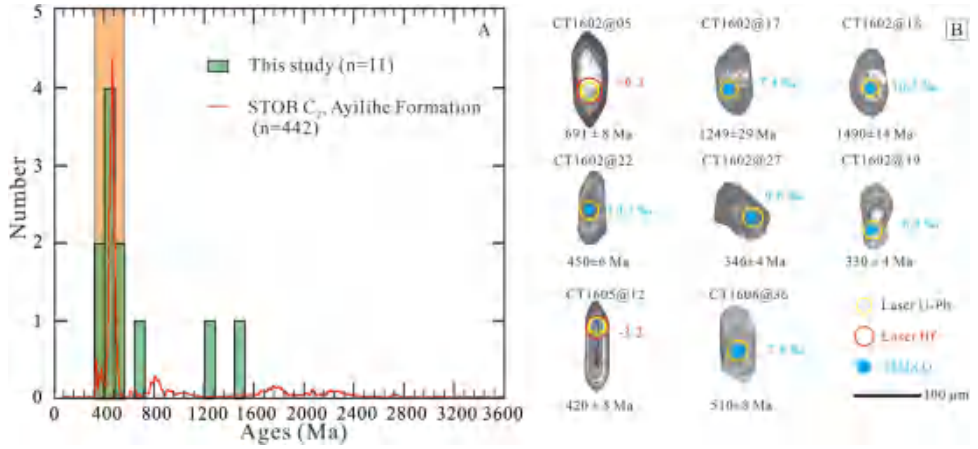

Fig. 6. (A) Histogram of U-Pb ages for inherited zircon cores from the late Carboniferous granitoids; (B) Representative cathodoluminescence (CL) images of zircon from the late Carboniferous granitoids. The data sources for rocks in the Ayilihe Formation are from Han and others, (2016a, 2016b).

cores, respectively (figs. 5 and 6). Zircons from muscovite-bearing granitoids (sample CT1605) and biotite granitoids (sample CT1606) show well-defined oscillatory zoning and high Th/U ratios (0.18–1.18) indicating a magmatic origin (Belousova and others, 2002). The zircon rims from samples CT1605 and CT1606 yielded $^{206}Pb/^{238}U$ ages of 291 to 305 Ma and 286 to 312 Ma, with weighted-mean ages of 299 6 2 Ma (1 r; MSWD = 0.47; fig. 5A) and "299 6 3" Ma (1 r; MSWD = 2.6; fig. 5B), respectively. Furthermore, U-Pb ages for the inherited zircon cores from two granitoid samples vary from 330 to 1490 Ma (table 2), with major clusters at 400 to 500 Ma (fig. 6A).

Major and Trace Element Geochemistry

Whole-rock major and trace element compositions are given in table 3. The muscovite-bearing granitoids have higher SiO_2 contents (70.9–74.7 wt.%) and lower TiO_2 (0.16–0.30 wt.%), Fe_2O_3 (1.04–1.84 wt.%), MgO (0.33–0.66 wt.%) and CaO contents (0.87–1.85 wt.%) than those of the biotite granitoids (table 3). All samples have high K_2O (3.50–5.17 wt.%) contents (fig. 7A), with alkali-calcic and calc-alkalic characteristics (fig. 7B). On the total alkali-silica (TAS) diagram (fig. 7C), all muscovite-bearing granitoid samples fall in the granite field, whereas the biotite granitoids plot in the quartz monzonite and granite field. On an A/NK vs A/CNK diagram (fig. 7D; Maniar and Piccoli, 1989), both the biotite granitoids and muscovite-bearing granitoids have low A/CNK ratios (1.0–1.1), most of which are <1.1, indicating weakly peraluminous compositions.

The muscovite-bearing granitoids have low REE contents, and show variable enriched LREE patterns ($(La/Yb)_N$ = 4.81–28.8) and significant negative Eu anomalies (fig. 8A; Eu/Eu* = 0.34–0.63). In contrast, the biotite granitoids have higher REE contents, more enriched LREE patterns ($(La/Yb)_N$ = 24.5–34.0) with moderate negative Eu anomalies (fig. 8A; Eu/Eu* = 0.67–0.73). On a primitive mantle-normalized plot (fig. 8B), all samples are enriched in large ion lithophile elements (LILE), such as Rb, Th and K, and have depleted high field strength elements (HFSE), such as Nb, Ta and Ti.

TABLE 3

Major (wt.%) and trace element (ppm) data of granitoid rocks in the South Tianshan

Rock type	Biotite granitoids										Muscovite-bearing granitoids						
Sample No.	CT16 02-1*	CT160 2-2*	CT16 02-3*	CT16 02-4*	CT16 02-5*	CT16 06-1	CT16 06-2	CT16 06-3	CT16 06-4	CT16 06-5	CT160 4-1	CT160 4-2	CT16 05-1	CT16 05-2	CT16 05-3	CT16 05-4	CT16 05-5
Major elements (wt.%)																	
SiO_2		69.30	68.40	70.10	70.30	66.60	66.80	65.80	67.20	67.60	74.70	73.30	74.40	71.10	72.10	70.90	71.40
Al_2O_3		14.80	15.80	14.50	14.40	15.70	15.60	15.80	15.30	15.70	13.50	13.50	13.50	15.20	14.80	15.00	14.90
Na_2O		3.50	3.46	3.65	3.25	3.33	3.42	3.41	3.36	3.36	3.61	3.51	3.50	3.68	3.88	3.97	3.67
MgO		1.07	0.89	1.01	0.92	1.53	1.50	1.67	1.35	1.37	0.33	0.33	0.65	0.60	0.66	0.66	0.63
K_2O		4.40	5.31	3.85	4.70	4.52	4.48	4.15	4.72	4.70	4.70	5.02	3.50	5.17	3.80	4.61	4.26
CaO		2.18	2.00	2.23	1.90	2.80	2.74	2.94	2.63	2.58	0.87	0.96	1.54	1.56	1.85	1.77	1.73
MnO		0.04	0.05	0.04	0.03	0.05	0.05	0.05	0.05	0.04	0.04	0.03	0.03	0.02	0.03	0.03	0.03
Fe_2O_3		3.17	2.50	3.00	2.67	3.42	3.41	3.76	3.16	3.18	1.04	1.07	1.80	1.68	1.84	1.76	1.79
TiO_2		0.55	0.45	0.55	0.47	0.68	0.66	0.74	0.61	0.61	0.17	0.16	0.29	0.27	0.30	0.30	0.29
P_2O_5		0.23	0.26	0.22	0.20	0.22	0.22	0.24	0.20	0.20	0.09	0.09	0.06	0.14	0.15	0.16	0.16
LOI		0.56	0.57	0.57	0.52	0.45	0.68	0.89	0.98	0.51	0.45	1.44	0.45	0.40	0.38	0.42	0.47
Total		99.80	99.70	99.70	99.40	99.40	99.60	99.40	99.60	99.80	99.50	99.30	99.80	99.80	99.80	99.60	99.40
K_2O+Na_2O		7.91	8.78	7.49	7.95	7.85	7.90	7.56	8.08	8.06	8.31	8.52	7.00	8.84	7.68	8.58	7.93
K_2O/Na_2O		1.26	1.53	1.05	1.44	1.36	1.31	1.22	1.41	1.40	1.30	1.43	1.00	1.40	0.98	1.16	1.16
A/CNK		1.02	1.04	1.02	1.04	1.02	1.01	1.02	0.99	1.02	1.07	1.04	1.10	1.05	1.07	1.02	1.08
A/NK		1.40	1.37	1.42	1.38	1.52	1.49	1.56	1.44	1.47	1.23	1.20	1.42	1.30	1.41	1.30	1.40
Trace elements (ppm)																	
Sc	11.00	9.51	8.7	9.3	8.43	8.56	9.43	9.15	8.52	8.23	5.22	5.59	5.99	6.08	6.44	6.1	6.24
V	59.8	48.7	40.9	45.8	41.1	60.3	60.5	67.6	52.9	55.3	10.3	10.5	22.7	21	23.4	23.1	23.7
Cr	16.2	14.7	12.1	13.2	12.3	24	34.5	25.5	26.7	20.2	3.82	3.59	10.6	5.94	7.08	7.55	7.31
Co	7.32	6.21	5.54	5.95	5.32	7.76	8.08	8.99	6.75	7.23	1.45	1.46	3.11	2.86	3.07	3.09	3.21
Ni	8.26	8.64	6.53	6.92	5.99	10.70	15.50	11.00	11.50	8.10	2.04	2.09	5.62	3.26	3.24	3.80	4.40
Ga	19.6	20.3	19.8	20	18.8	21.7	22.2	22.7	20.8	21.5	17.5	18.2	18.3	18.5	19	19.3	18.5
Rb	195	212	219	195	212	194	218	193	207	209	249	258	161	188	151	178	176
Sr	178	226	241	220	214	327	327	334	311	316	61.5	57.9	189	203	196	233	201
Y	22.8	22.2	23.7	20.1	19.6	11.6	11.2	12.6	12.9	12.6	13.8	18.4	5.4	7.2	8.5	7.9	8.3
Zr	236	235	220	228	200	217	221	253	232	209	121	74	98	114	111	101	107
Nb	19.1	16.4	14.9	16.4	14.4	10.6	10.7	11.9	10.3	10.6	17.6	16.6	10.1	9.6	9.2	9.2	10.4
Ba	270	564	755	466	624	700	708	694	675	714	171	168	420	731	464	678	538
La	53.7	46.9	46.4	45.2	38.2	31	40.7	32.6	38.2	43.3	16	16.1	20.7	17.6	21.6	20.1	19.6
Ce	109.0	94.7	94.1	91.4	77.6	63.8	82.2	67.9	78.1	88.0	34.8	35.3	40.9	35.9	43.9	41.6	39.6
Pr	11.80	10.20	10.30	9.89	8.45	6.94	8.76	7.24	8.41	9.46	3.85	3.93	4.26	3.82	4.69	4.52	4.37

TABLE 3
(continued)

Rock type	Biotite granitoids										Muscovite-bearing granitoids						
Sample No.	CT16 02-1*	CT160 2-2*	CT16 02-3*	CT16 02-4*	CT16 02-5*	CT16 06-1	CT16 06-2	CT16 06-3	CT16 06-4	CT16 06-5	CT160 4-1	CT160 4-2	CT16 05-1	CT16 05-2	CT16 05-3	CT16 05-4	CT16 05-5
Trace elements (ppm)																	
Nd	43.5	37.5	38.7	36.5	31.2	27.1	32.3	28.6	31.5	35.1	14.3	14.1	15.6	14.0	17.3	16.4	15.7
Sm	7.53	6.60	6.92	6.26	5.79	4.67	5.02	5.00	5.24	5.61	2.91	3.04	2.78	2.62	3.53	3.13	3.17
Eu	0.83	1.04	1.03	0.94	0.96	1.00	1.06	1.06	1.03	1.08	0.32	0.32	0.49	0.52	0.54	0.59	0.55
Gd	5.57	5.08	5.30	4.84	4.16	3.49	3.55	3.85	3.79	3.86	2.24	2.48	1.95	2.21	2.62	2.29	2.58
Tb	0.84	0.78	0.84	0.74	0.68	0.47	0.47	0.51	0.53	0.52	0.42	0.47	0.26	0.35	0.40	0.34	0.38
Dy	3.91	3.95	4.29	3.66	3.44	2.11	2.09	2.40	2.32	2.28	2.45	3.05	1.14	1.67	1.83	1.71	1.85
Ho	0.83	0.82	0.94	0.75	0.74	0.45	0.38	0.45	0.48	0.47	0.51	0.69	0.20	0.29	0.35	0.33	0.34
Er	2.17	2.33	2.40	2.08	2.04	1.07	1.09	1.15	1.22	1.18	1.47	2.00	0.53	0.71	0.90	0.83	0.84
Tm	0.30	0.31	0.34	0.25	0.29	0.13	0.14	0.16	0.17	0.16	0.25	0.34	0.07	0.10	0.11	0.12	0.11
Yb	2.07	2.13	2.19	1.93	1.84	0.91	0.86	0.93	1.06	1.05	1.72	2.4	0.52	0.70	0.73	0.75	0.77
Lu	0.32	0.31	0.33	0.26	0.27	0.12	0.14	0.14	0.16	0.14	0.27	0.36	0.09	0.10	0.12	0.11	0.11
Hf	6.85	6.65	6.51	7.00	6.16	5.28	5.76	6.34	6.25	5.42	4.37	2.89	3.10	3.83	3.87	3.39	3.61
Ta	2.22	1.95	1.77	2.17	1.72	0.68	0.62	0.71	0.89	0.86	2.72	2.45	1.30	1.48	1.41	1.45	1.67
Th	32.3	27.4	27.2	26.7	23.0	17.2	23.6	20.5	23.0	27.4	14.7	14.9	11.7	10.6	12.8	11.7	11.5
U	3.21	4.25	6.57	3.03	2.87	1.37	1.99	1.51	3.17	3.31	3.78	4.09	2.13	2.68	3.68	1.86	2.12
Eu/Eu*	0.38	0.53	0.5	0.5	0.57	0.73	0.73	0.71	0.68	0.67	0.37	0.35	0.61	0.64	0.52	0.64	0.57
LREE	226.0	197.0	197.0	190.0	162.0	135.0	170.0	142.0	162.0	183.0	72.2	72.8	84.7	74.5	91.6	86.3	83.0
ΣREE	242.0	213.0	214.0	205.0	176	143	179	152	172	192.0	81.5	84.6	89.5	80.6	98.6	92.8	90.0
Zr+Nb+Ce+Y	387	368	353	356	312	303	325	345	333	320	187	144	155	167	173	160	165
$(La/Yb)_N$	18.6	15.8	15.2	16.8	14.9	24.5	34.0	25.2	25.8	29.6	6.7	4.8	28.8	18.0	21.3	19.3	18.4
T_{Zr}		809	811	805	803	786	788	795	794	790	789	743	757	766	759	749	758

A/CNK= molar $Al_2O_3/(CaO+Na_2O+K_2O)$; T_{Zr} = zircon saturation temperature.
* The data are from Tao and others (2019).

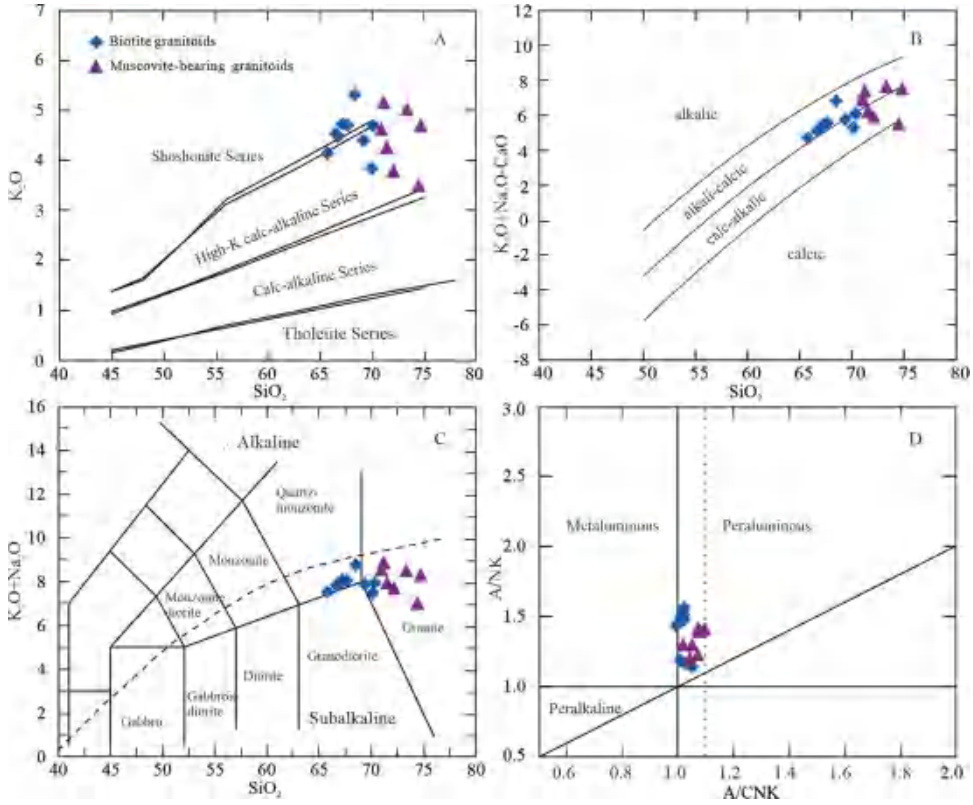

Fig. 7. (A) K_2O vs. SiO_2 diagram (after Gill, 1981); (B) (Na_2O+K_2O-CaO) vs. SiO_2 (after Frost and others, 2001); (C) Total alkalis vs. silica diagram (after Middlemost, 1994); (D) A/NK vs. A/CNK diagram (After Maniar and Piccoli, 1989).

Whole Rock Sr-Nd Isotopic Compositions

The whole rock Sr-Nd isotopic results are presented in table 4. The biotite granitoids and muscovite-bearing granitoids have a wide range of $^{87}Rb/^{86}Sr$ ratios between 1.71 and 12.88, and high initial $^{87}Sr/^{86}Sr$ ratios from 0.7080 to 0.7188. These rocks

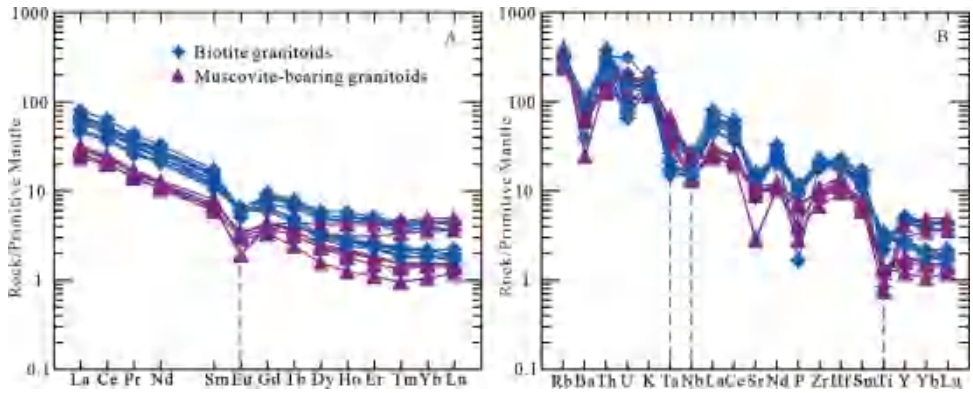

Fig. 8. (A) primitive mantle-normalized REE patterns, (B) primitive mantle-normalized spidergram of granitoids from the Hejing region in the STOB (normalization values from Sun and McDonough, 1989).

TABLE 4

Whole-rock Sr-Nd isotopic compositions of granitoid rocks in the Southern Tianshan

Sample No.	$^{87}Rb/^{86}Sr$	$^{87}Sr/^{86}Sr$	±2σ	$(^{87}Sr/^{86}Sr)_i$	$^{147}Sm/^{144}Nd$	$^{143}Nd/^{144}Nd$	±2σ	$\varepsilon Nd_{(t)}$	T_{DM} (Ma)	T_{2DM} (Ma)
Biotite granitoids										
CT1602-1*	3.167	0.722486	0.000012	0.7092	0.1046	0.512187	0.000006	-5.3	1347	1495
CT1602-2*	2.712	0.725624	0.000013	0.7142	0.1063	0.512567	0.000007	2	831	896
CT1606-1	1.715	0.715395	0.000014	0.708	0.1041	0.51218	0.000007	-5.4	1351	1504
CT1606-2	1.927	0.716448	0.000011	0.7081	0.0939	0.512137	0.000007	-5.8	1291	1540
Muscovite-bearing granitoids										
CT1604-1	11.706	0.762557	0.000017	0.7133	0.123	0.512198	0.000006	-5.8	1601	1534
CT1604-2	12.883	0.772987	0.000012	0.7188	0.1303	0.512228	0.000006	-5.5	1686	1508
CT1605-1	2.463	0.719115	0.000013	0.7086	0.1077	0.512075	0.000007	-7.6	1547	1682
CT1605-2	2.678	0.720624	0.000014	0.7092	0.1131	0.512119	0.000008	-6.9	1563	1629

* The data are from Tao and others (2019).

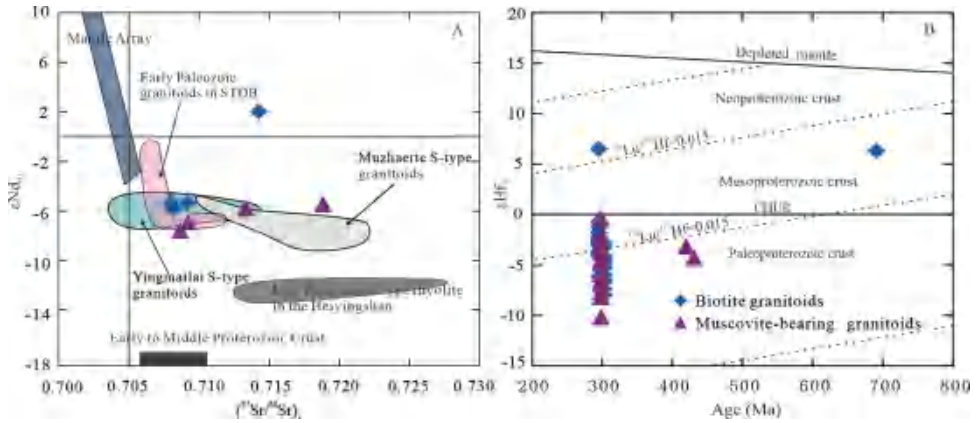

Fig. 9. (A) Nd-Sr isotopic compositions; Date sources: early Paleozoic granitoids from the STOB are from Kong and others (2019), the Heiyingshan S-type rhyolite data from Cheng and others (2017), Muzhaierte S-type granitoids from Gou and others (2015), Yingmailai S-type granitoids from Ma and others (2010). (B) eHf(t) vs. Age plot of the granitoids rocks.

have negative eNd(t) values of −5.3 to −7.6, except for sample CT1602-2, which was a positive eNd(t) ratio of 12.0 (fig. 9A).

Zircon Hf-O Isotopic Compositions

The zircon Lu-Hf and O isotopic data for the studied granitoids are given in tables 5 and 6, respectively. Zircon rims from these granitoids have variable eHf(t) values (−10.2 to −0.35) and old Hf model ages (1.34–1.96 Ga), except for one spot (CT1602@11), which has a positive eHf(t) value of 16.48 and younger Hf model age of 0.90 Ga. However, the inherited zircon cores have relatively variable eHf(t) values of −4.3 to 16.3 compared to the rims (fig. 9B). The zircons rims also show coherently high $\delta^{18}O_{zrn}$ values of 8.9 to 11.7 ‰ (fig. 10), with an average value of 10.3 6 0.3 ‰ (1SD). However, the inherited zircons cores have relatively lower $\delta^{18}O_{zrn}$ of 6.3 to 10.5 ‰ (fig. 10).

discussion

Geochemical Affinities

The late Carboniferous granitoids from the STOB have peraluminous characteristics, with A/CNK values of 1.0 to 1.1. However, they have been variously classified as I-type, A-type and S-type granitoid rocks. Firstly, the late Carboniferous granitoids have low $(K_2O + Na_2O)/Al_2O_3$, FeO^T/MgO, and Ga/Al ratios and Zr, Hf and Ga contents (fig. 11A) and do not contain any alkaline mafic minerals, precluding that they belong to A-types. Secondly, these granitoids show P_2O_5 contents that decrease with increasing SiO_2 content (fig.11B) and A/CNK values that rise slightly with increasing SiO_2 (fig. 11C). These features seem to be similar to those of typical I-type granites as defined by White and Chappell (1977) in the Lachlan Fold Belt. However, all granitoids have high K_2O/Na_2O ratios of 0.98 to 1.53 (table 3), initial $^{87}Sr/^{86}Sr$ ratios of 0.7080 to 0.7188, and low eNd(t) values of −5.3 to −7.6 (fig. 9A), as well as zircon eHf (t) values of −10.2 to −0.77 (fig. 9B). These geochemical features are consistent with the characteristics of common S-type granitoids (Chappell and White, 1974; McCulloch and Chappell, 1982). Therefore, the geochemical characteristics have little capacity to identify the source nature of the studied granitoids.

TABLE 5

Zircon Hf isotope data of granitoid rocks in the South Tianshan

Analysis spot	Age	$^{176}Yb/^{177}Hf$ (corr)	$^{176}Lu/^{177}Hf$ (corr)	2σ	$^{176}Hf/^{177}Hf$ (corr)	2σ	fLu/Hf	εHf(t)	T_{DM1} (Ma)	T_{DM2} (Ma)
Biotite granitoid (CT1602)										
CT1602@1*	295.8	0.023760	0.000970	0.000102	0.282488	0.000022	-0.97	-3.74	1080	1551
CT1602@2*	295.8	0.035599	0.001453	0.000154	0.282535	0.000025	-0.96	-2.18	1027	1452
CT1602@3*	295.8	0.031813	0.001283	0.000255	0.282479	0.000021	-0.96	-4.11	1101	1575
CT1602@4*	295.8	0.030158	0.001219	0.000477	0.282521	0.000022	-0.96	-2.61	1040	1480
CT1602@5*	691	0.031865	0.001256	0.000209	0.282535	0.000024	-0.96	6.30	1021	1221
CT1602@6*	295.8	0.038127	0.001525	0.000410	0.282522	0.000024	-0.95	-2.64	1047	1481
CT1602@7*	295.8	0.037034	0.001484	0.000267	0.282483	0.000025	-0.96	-4.01	1101	1568
CT1602@8*	295.8	0.027509	0.001115	0.000261	0.282479	0.000022	-0.97	-4.09	1096	1573
CT1602@9*	295.8	0.030870	0.001248	0.000098	0.282515	0.000021	-0.96	-2.82	1049	1493
CT1602@10*	295.8	0.035349	0.001396	0.000295	0.282545	0.000026	-0.96	-1.79	1010	1428
CT1602@11*	295.8	0.034425	0.001346	0.000149	0.282779	0.000025	-0.96	6.48	677	901
CT1602@12*	295.8	0.042437	0.001695	0.000666	0.282423	0.000030	-0.95	-6.18	1193	1705
CT1602@13*	295.8	0.039648	0.001582	0.000330	0.282561	0.000027	-0.95	-1.26	993	1394
CT1602@14*	295.8	0.041417	0.001626	0.000653	0.282513	0.000024	-0.95	-2.97	1063	1503
CT1602@15*	295.8	0.046428	0.001836	0.000220	0.282577	0.000030	-0.94	-0.77	977	1363
CT1602@16*	295.8	0.038911	0.001559	0.000110	0.282528	0.000020	-0.95	-2.45	1040	1470
Muscovite-bearing granitoid (CT1605)										
CT1605@1	298.5	0.025239	0.001013	0.000288	0.282462	0.000019	-0.97	-4.61	1118	1608
CT1605@2	298.5	0.041046	0.001626	0.000238	0.282485	0.000020	-0.95	-3.89	1102	1563
CT1605@3	298.5	0.013806	0.000533	0.000144	0.282421	0.000018	-0.98	-5.96	1160	1694
CT1605@4	298.5	0.015944	0.000684	0.000202	0.282404	0.000020	-0.98	-6.57	1188	1732
CT1605@5	298.5	0.035535	0.001389	0.000120	0.282494	0.000018	-0.96	-3.53	1083	1540
CT1605@6	298.5	0.027859	0.001117	0.000356	0.282375	0.000022	-0.97	-7.70	1243	1803
CT1605@7	298.5	0.018728	0.000750	0.000374	0.282514	0.000022	-0.98	-2.72	1037	1489
CT1605@8	298.5	0.029285	0.001171	0.001064	0.282305	0.000029	-0.96	-10.18	1343	1959
CT1605@9	431	0.020122	0.000915	0.000631	0.282389	0.000018	-0.97	-4.31	1216	1693
CT1605@10	298.5	0.028828	0.001131	0.000298	0.282536	0.000020	-0.97	-1.99	1016	1443
CT1605@11	298.5	0.009978	0.000323	0.000883	0.282356	0.000023	-0.99	-8.22	1244	1836
CT1605@12	420	0.055764	0.002246	0.001140	0.282438	0.000021	-0.93	-3.21	1190	1615
CT1605@13	298.5	0.050291	0.001977	0.000294	0.282399	0.000030	-0.94	-7.01	1237	1760
CT1605@14	298.5	0.023405	0.000941	0.000209	0.282463	0.000024	-0.97	-4.55	1114	1605
CT1605@15	298.5	0.013046	0.000526	0.000060	0.282453	0.000019	-0.98	-4.80	1115	1621
CT1605@16	298.5	0.013997	0.000569	0.000065	0.282397	0.000020	-0.98	-6.80	1194	1747
CT1605@17	298.5	0.030941	0.001325	0.000587	0.282584	0.000024	-0.96	-0.35	954	1339
Biotite granitoid (CT1606)										
CT1606@1	302.6	0.014252	0.000584	0.000050	0.282461	0.000015	-0.98	-4.44	1105	1601
CT1606@2	302.6	0.022755	0.000946	0.000365	0.282448	0.000024	-0.97	-5.00	1135	1636
CT1606@3	302.6	0.021400	0.000859	0.000223	0.282406	0.000025	-0.97	-6.48	1192	1729
CT1606@4	302.6	0.014570	0.000602	0.000154	0.282494	0.000017	-0.98	-3.28	1060	1527
CT1606@5	302.6	0.016447	0.000687	0.000179	0.282361	0.000022	-0.98	-8.01	1248	1826
CT1606@6	302.6	0.016543	0.000672	0.000102	0.282397	0.000036	-0.98	-6.73	1197	1745
CT1606@7	302.6	0.016546	0.000676	0.000153	0.282449	0.000017	-0.98	-4.91	1126	1630
CT1606@8	302.6	0.017247	0.000689	0.000082	0.282379	0.000030	-0.98	-7.40	1224	1787
CT1606@9	302.6	0.016035	0.000657	0.000287	0.282454	0.000023	-0.98	-4.71	1118	1618
CT1606@10	302.6	0.012980	0.000528	0.000091	0.282448	0.000024	-0.98	-4.89	1122	1629
CT1606@11	302.6	0.019403	0.000850	0.000056	0.282418	0.000018	-0.97	-6.03	1174	1701
CT1606@12	302.6	0.018395	0.000735	0.000345	0.282507	0.000021	-0.98	-2.85	1046	1501
CT1606@13	302.6	0.016073	0.000687	0.000077	0.282418	0.000019	-0.98	-5.99	1169	1699
CT1606@14	302.6	0.016454	0.000682	0.000240	0.282438	0.000023	-0.98	-5.28	1140	1654
CT1606@15	302.6	0.017159	0.000698	0.000210	0.282451	0.000017	-0.98	-4.84	1123	1626
CT1606@16	302.6	0.015312	0.000640	0.000066	0.282472	0.000017	-0.98	-4.10	1093	1579

* The data are from Tao and others (2019).

TABLE 6

Zircon O isotopic compositions of granitoid rocks in the South Tianshan

Sample spot	Ages (Ma)	Intensity O16	O^{18}/O^{16} Mean	$\delta^{18}O$(‰)	2SE
Biotite granitoid (CT1602)					
CT1602@17	1249	1499160000	0.002029	7.41	0.28
CT1602@18	1490	1493858000	0.002035	10.45	0.30
CT1602@19	330	1499399000	0.002027	6.34	0.29
CT1602@20	306	1482892000	0.002034	9.69	0.31
CT1602@21	310	1499205000	0.002035	10.39	0.17
CT1602@22	450	1491158000	0.002035	10.33	0.20
CT1602@23	298	1103074000	0.002034	9.97	0.42
CT1602@24	318	1505986000	0.002034	9.69	0.26
CT1602@25		1516307000	0.002033	9.28	0.16
CT1602@26		1517093000	0.002034	9.86	0.19
CT1602@27	346	1537826000	0.002034	9.61	0.27
CT1602@28		1532076000	0.002032	8.87	0.29
CT1602@29		1542315000	0.002035	10.32	0.29
CT1602@31		1532220000	0.002033	9.43	0.21
Biotite granitoid (CT1606)					
CT1606@26	295	1222428000	0.002037	11.04	0.22
CT1606@27	293	1224085000	0.002037	10.63	0.32
CT1606@30	281	1544996000	0.002036	10.60	0.25
CT1606@31	330	1550986000	0.002036	10.54	0.23
CT1606@32	286	1560702000	0.002036	10.80	0.27
CT1606@33	288	1568424000	0.002036	10.84	0.22
CT1606@34	311	1560350000	0.002036	10.81	0.20
CT1606@35		1509094000	0.002036	10.54	0.24
CT1606@36	510	1533355000	0.002030	7.80	0.30
CT1606@37		1495308000	0.002036	10.82	0.28
CT1606@38	286	1536099000	0.002036	10.77	0.24
CT1606@39		1487026000	0.002036	10.71	0.28
CT1606@40	291	1464762000	0.002038	11.74	0.24

In contrast, O isotopic data are effective in tracing the involvement of material that has experienced surface processes in the source (Valley, 2003; Kemp and others, 2007). The studied granitoids have higher $d^{18}O_{zrn}$ values of 8.87 to 11.74 ‰ (fig.10) than those of typical I-type granitoids that have $d^{18}O_{zrn}$ values ranging from 5 ‰ to 8.5 ‰ (Kemp and others, 2009; Gao and others, 2014). Such high $d^{18}O_{zrn}$ values are common in S-type granitoids elsewhere in the world, such as the Bhutan leucogranites in the eastern Himalayan orogen (Hopkinson and others, 2017), and Neoproterozoic S-type granitoids in the Alxa Block (Dan and others, 2014). Furthermore, the muscovite-bearing granitoids contain strongly peraluminous minerals such as muscovite, but lack hornblende, which is also consistent with the mineralogical characteristics of typical S-type granitoids (Chappell and White, 2001). As a result, the studied granitoids in the STOB are best categorized as being weakly peraluminous S-type granitoids.

Origin of Inherited Zircon Cores

Most of the studied zircon grains from late Carboniferous S-type granitoids of the STOB contain cores that are texturally discordant to their thick rims. These inherited zircon cores gave ages of 1490 to 330 Ma, with relatively lower O compositions ($d^{18}O_{zrn}$= 6.34–10.5 ‰; table 6) than those of zircon rims, and a distinct age peak between 400 to 500 Ma (fig. 6A). These inherited zircons could potentially be

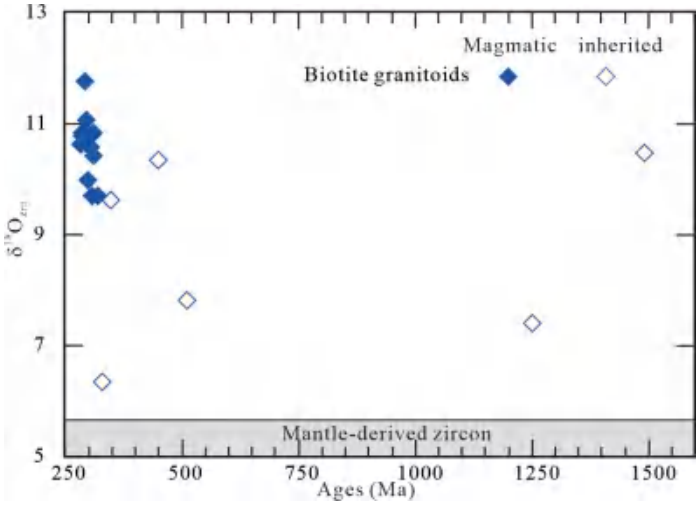

Fig. 10. Plot of $\delta^{18}O_{zrn}$ values for the late Paleozoic biotite granitoids in the STOB, the field of mantle-derived zircons is from Valley and others (1998).

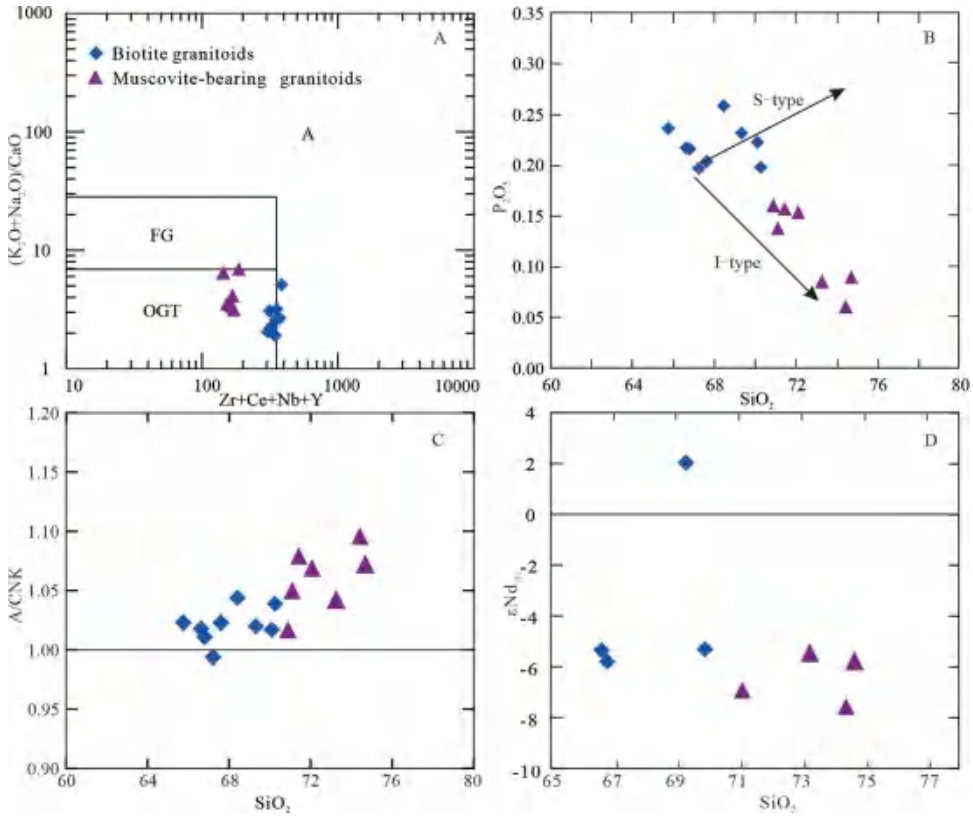

Fig. 11. (A) $(K_2O+Na_2O)/CaO$ vs. Zr+Ce+Nb+Y discrimination diagram (Whalen and others, 1987); (B) P_2O_5 vs. SiO_2 diagram, the trend of I- and S-type granitoids follows Chappell (1999); (C) A/CNK vs. SiO_2; (D) $\varepsilon Nd(t)$ vs. SiO_2 diagram.

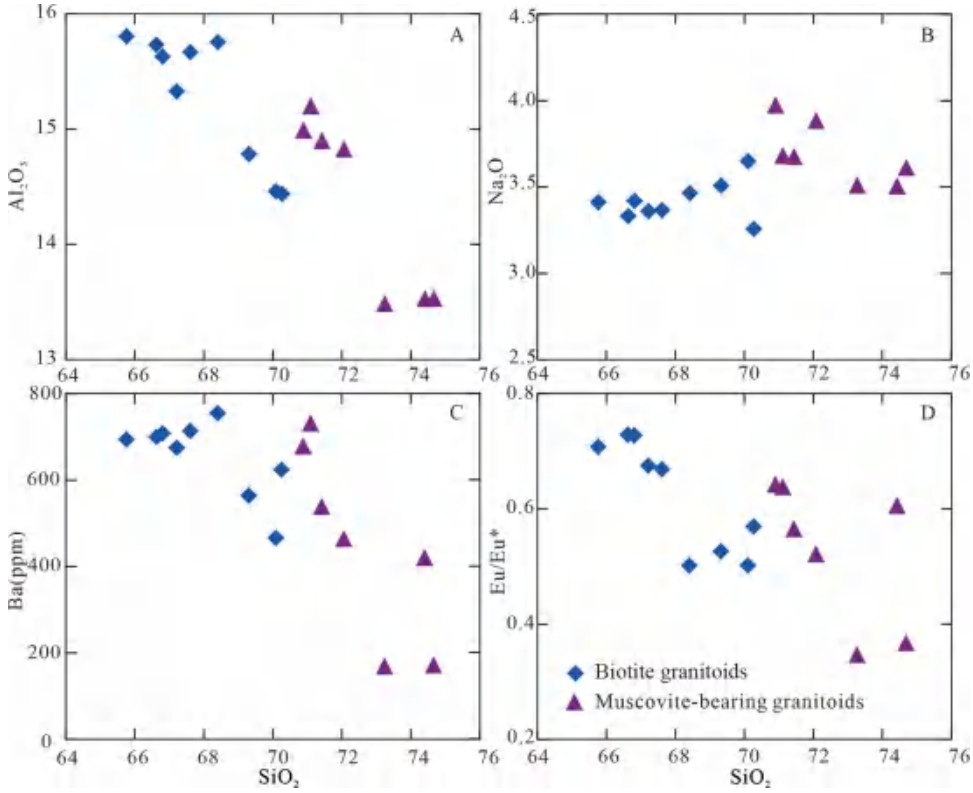

Fig. 12. Harker plots of major elements and trace elements for the late Carboniferous granitoids from the STOB.

xenocrysts assimilated from crustal country rocks during emplacement of granitic magmas. However, field geology shows no clear evidence of crustal assimilation because no xenoliths of the country rocks have been observed in the studied S-type granitoids (fig. 3). Besides, whole-rock Nd isotopes show relatively limited variations and do not change with increasing SiO_2 contents (fig. 11D). Therefore, the inherited zircons could be inherited from crustal sources rather than assimilated from the country rocks as xenocrysts.

The U-Pb ages of inherited zircon cores show large variations (fig. 6A). Such an age distribution is consistent with typical S-type granitoids (Gao and others, 2016). In addition, these rocks show high zircon $\delta^{18}O$ values of 8.78 to 11.7 ‰ (fig. 10) significantly higher than those of igneous zircons from low crustal-derived magmas (5‰–7.5‰; Valley and others, 2005), suggesting these rocks were most likely sourced from sedimentary rocks (δ^{18O} >8 ‰; Valley and others, 2005; Kemp and others, 2007). Furthermore, inherited zircon derived directly from the source rocks provides accurate detrital zircon age information (Jeon and others, 2014; Yu and others, 2019a, 2019b). The ages of the youngest inherited zircon place an upper limit on the depositional age of these metasedimentary source rocks. The youngest inherited detrital zircon core age of ; 330 Ma is consistent with a late Carboniferous depositional age for these sedimentary rocks (for example, Ayilihe Formation) in the STOB (fig. 6A; Han and others, 2016a, 2016b). Therefore, these data indicate

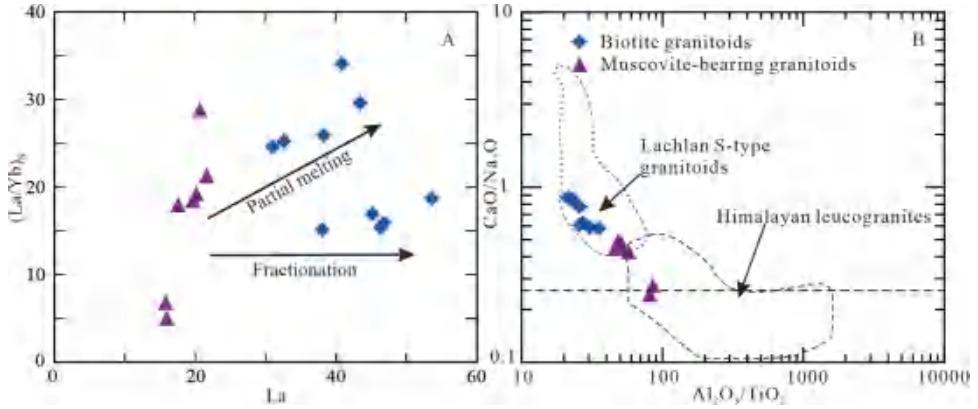

Fig. 13. (A) Plot of $(La/Yb)_N$ vs. La, showing partial melting and fractionation trends; (B) Chemical composition of late Carboniferous granitoids compared with Lachlan S-type granitoids and Himalayan leucogranites. Data sources are: Lachlan S-type granitoids from White and Chappell (1988), Chappell and White (1992); Himalayan leucogranites from Visona and Lombardo (2002), Zhang and others (2004) and Guo and Wilson (2012).

that the studied S-type granitoids likely originated from the melting of late Carboniferous sedimentary rocks (Han and others, 2016a, 2016b).

Source and Petrogenesis of S-Type Granitoids

Compared to typical S-type granitoids, the S-type granitoids in this study exhibit more variable CaO/FeO^T ratios (0.62–0.91), lower A/CNK values (1.0 to 1.1; table 3) and lower P_2O_5 contents (0.09 to 0.26 wt.%) (Chappell and others, 1987). In addition, the negative correlation between whole-rock P_2O_5 and SiO_2 is a feature more typical of I-type granitoids (fig. 11B). Therefore, it is intriguing why some S-type granitoids show geochemistry more characteristic of the transition between I- and S-type granitoids and even I-type granitoids. In other studies with similar results, various models have been proposed to explain this phenomenon such as the composition of source rocks, partial melting conditions, restite unmixing and peritectic assemblage entrainment processes, and magmatic processes (for example, magma mixing, fractional crystallization and assimilation of country rocks; Kemp and others, 2007; Clemens and Stevens, 2012; Zhao and others, 2015; Gao and others, 2014, 2016).

Firstly, the S-type granitoids in this study do not contain residual or peritectic minerals, such as garnet or cordierite, indicating that restite unmixing and peritectic minerals entrainment did not contribute to the chemical variations of these granitoids. Secondly, contributions from mantle-derived magma are readily excluded, because mafic microgranular enclaves and coeval mafic igneous rocks are absent in the study region. Thirdly, there are limited variations in whole-rock $\varepsilon Nd(t)$ values and $\delta^{18}O_{zrn}$ values within each sample. Therefore, they cannot be derived from either magma mixing or assimilation-fractional crystallization (AFC) processes.

Alternatively, peraluminous granitoids can be produced by the fractionation of mafic metaluminous magma (Zen, 1986). However, this process is not applicable to this study, as these granitoids are dominated by felsic compositions (67–75 wt.%), with a lack of mafic rocks and cumulates (fig. 1B). Additionally, many major and trace elements (for example, Al_2O_3, Na_2O, Ba and Eu/Eu*) behave scattered or stay constant with increasing SiO_2 (fig. 12), which also does not support fractional crystallization. Instead, these rocks show a typical trend of partial melting in the $(La/Yb)_N$ versus La

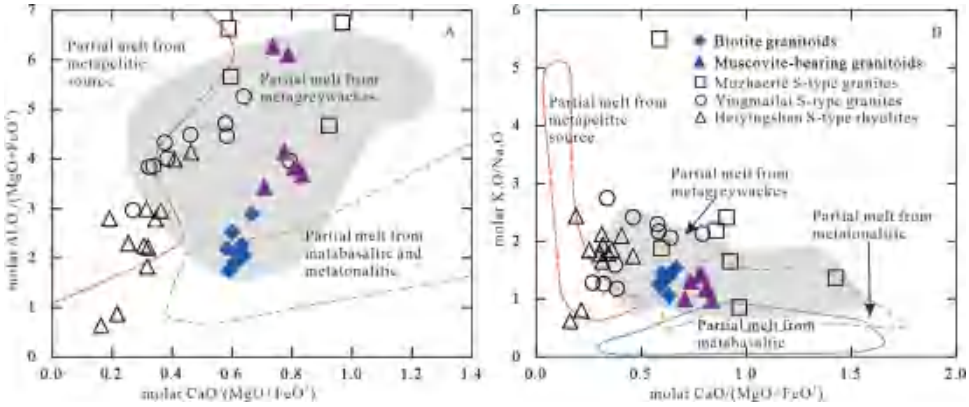

Fig. 14. (A) $Al_2O_3/(MgO + FeO^T)$ molar vs. $CaO/(MgO + FeO^T)$ molar diagram; (B) K_2O/Na_2O molar vs. $CaO/(MgO + FeO^T)$ molar diagram (Altherr and others, 2000; Altherr and Siebel, 2002). Data source for other S-type rocks are as in fig. 9.

diagram (fig. 13A), suggesting that partial melting may play an important role in the generation of these magmas.

Previous studies have confirmed that S-type granitoids are commonly produced by partial melting of metasedimentary rocks (Chappell and White, 1974), but some researchers (for example, Zhu and others, 2009) suggest that a few S-type granitoids contain mantle-derived materials and/or an intracrustal component (Appleby and others, 2010). The S-type granitoids in this study have obviously higher $\delta^{18}O_{zrn}$ values (. 8 ‰), than those of mantle-derived materials ($\delta^{18}O_{Zrn}$ = 5.3 6 0.3 ‰, Valley, 2003), suggesting that they were most likely generated by the partial melting of metasedimentary rocks. As argued above, the studied S-type granitoids likely originated from the partial melting of late Carboniferous sedimentary rocks such as the Ayilihe Formation. Although melt temperatures may affect the chemical variations of the S-type granitoids (Watson and Harrison, 1983), the granitoids display limited variations in whole-rock geochemical compositions (figs. 7 and 8; table 3). This means that the melting temperature did not play an important role in controlling the geochemical compositions of the S-type granitoids. Therefore, their geochemical and isotopic characteristics were primarily inherited from their sources. These granitoids show negative $\varepsilon Nd(t)$ values of (−7.6 to −5.3) with old Nd model ages (1.29 to 1.68 Ga) and negative zircon $\varepsilon Hf(t)$ values of (−10.2 to −0.35) with old Hf model ages (1.34 to 1.96 Ga), similar to those of metasedimentary rocks from Mesoproterozoic and upper Paleoproterozoic crustal materials. But the inherited zircons give younger source ages (330 to 1490 Ma), comparable with those of the detrital zircons from the sandstones of the late Carboniferous Ayilihe Formation (Li and others, 2014; Han and others, 2016a, 2016b). In addition, the zircon Lu-Hf isotopic analyses for the early Paleozoic inherited zircon cores yield two-stage Hf model ages of 1.22 to 1.69 Ga (fig. 9B; table 5), also similar to those of detrital zircons from late Carboniferous metasedimentary rocks (Han and others, 2016a), favoring these rocks as the main source rather than Mesoproterozoic and upper Paleoproterozoic crustal materials. Furthermore, previous studies have also found abundant Carboniferous inherited zircon grains in the late Carboniferous S-type granitoids of the STOB (Cheng and others, 2017), consistent with this study.

Petrologically, the source sandstones of the late Carboniferous Ayilihe Formation are characterized by relatively low textural and compositional maturity, with high lithic fragments (25.1%) and feldspar (7.52%; Li and others, 2014). Therefore, the

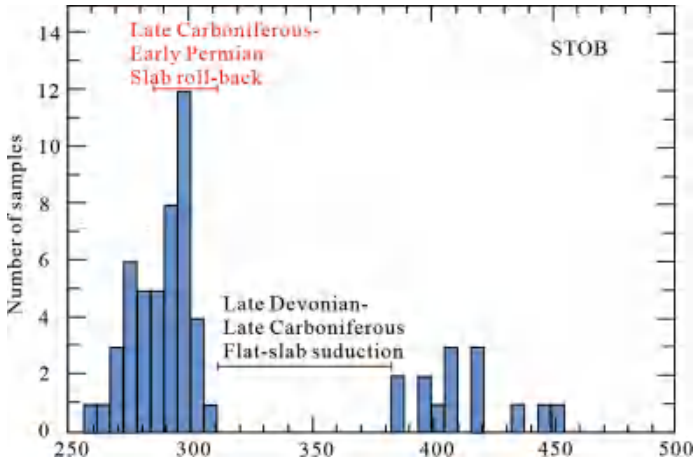

Fig. 15. Histogram of zircon U-Pb ages for granitoids of the STOB. Modified after Tao and others (2019).

studied S-type granitoids were derived from partial melting of the low compositional maturity metasedimentary rocks (plagioclase-rich, clay-poor source). They have chemical compositions similar to those of Lachlan S-type granitoids (fig. 13B; White and Chappell, 1988; Chappell and White, 1992), but different from those of Himalayan leucogranites which were dominantly produced by partial melting of pelitic rocks (fig. 13B; Visona and Lombardo, 2002; Zhang and others, 2004; Guo and Wilson, 2012). More recently, Gao and others (2014) concluded that the Luxi biotite granitoids with low A/CNK values (1.05 to 1.14, mostly < 1.1) belong to S-type granitoids, and were generated by partial melting of a relatively mafic metasedimentary rock, which was likely Al-poor but Ca-rich. Similarly, the S-type granitoids in this study are also weakly peraluminous, implying generation from low compositional maturity metasedimentary source (for example, metagraywackes; fig. 14A and B). It is well established that low compositional maturity metasedimentary rocks are enriched in feldspar and depleted in clay, and thus have a high content of Ca and Na, but low content of Al (Sylvester, 1998). Therefore, we emphasize that the high silica and weakly peraluminous features are largely controlled by source compositions, such as a low compositional maturity metasedimentary source. This mechanism also explains why the studied S-type granitoids not only show high $\delta^{18}O_{Zrn}$ values but also have other geochemical transitional features between I- and S-types granitoids.

In summary, we propose that the late Carboniferous low compositional maturity metasedimentary rocks were buried, heated and partially melted to produce the S-type granitoids. Therefore, it is inappropriate to categorize these granitoids using the A/CNK values and the variation trends in whole-rock P_2O_5 and A/CNK versus SiO_2. In contrast, zircon O isotopic compositions are useful in tracing the recycling of metasedimentary rocks (Kemp and others, 2007; Gao and others, 2016). As a result, the S-type granitoids do not necessarily show elevated A/CNK (. 1.1) values, but have high $\delta^{18}O_{Zrn}$ values.

Tectonic Implications

Late Carboniferous granitoids are widespread in the STOB, but it remains unclear whether these granitoids were formed in an arc-related setting (Zhang and others, 2007; Xiao and others, 2008, 2013) or in a post-collisional setting (Gao and

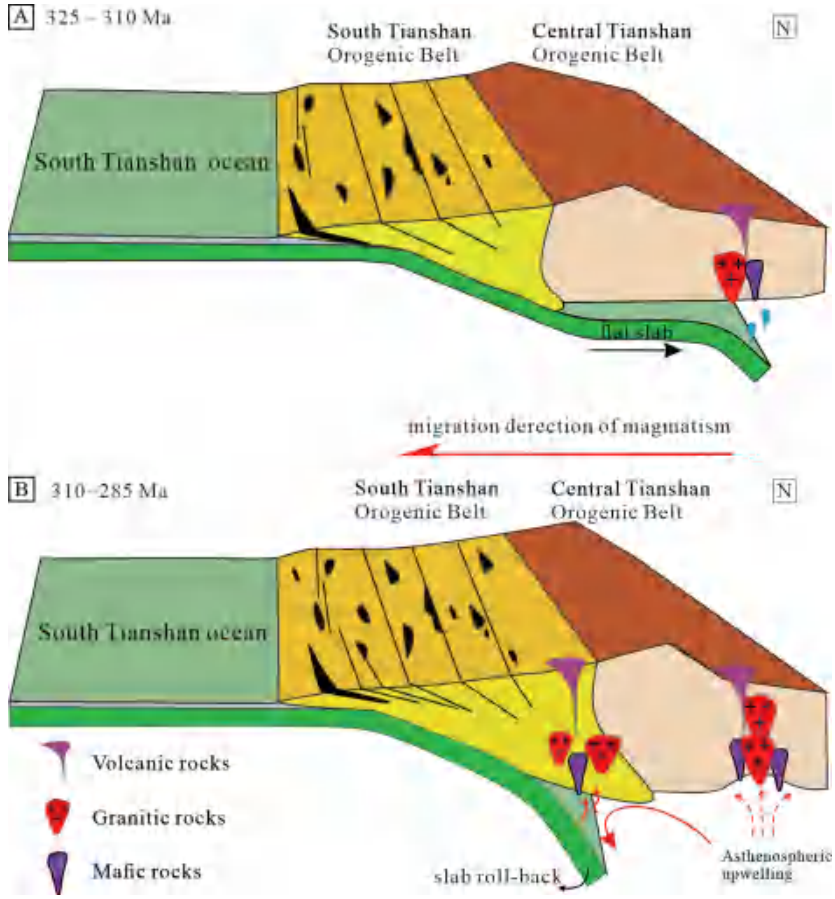

Fig. 16. Schematic cartoons illustrate the late Carboniferous to early Permian tectonic and magmatic evolution of the South Tianshan Ocean. Modified after Xiao and others (2013).

others, 2009; Han and others, 2011; Long and others, 2011). A mantle plume model has also been proposed to explain the genesis of the late Carboniferous magmatism in the STOB (Zhang and Zuo, 2013; Han and Zhao, 2018; Han and others, 2019). With regard to the plume model, studies of the plume-related Tarim large igneous province have revealed two magmatic pulses at 291 6 4 and 272 6 2 Ma, respectively (Tian and others, 2010). These magmatic rocks are mainly composed of A_1 or A_2 type granites. High temperature is one of the most remarkable features in these mantle plume-related granites (Zhang and others, 2008). However, the studied S-type granitoids of the STOB possess zircon saturation temperatures (Tzr = 743 to 814 °C) significantly lower than that of the granitoids related to the Emeishan plume (Tzr = 934 to 1053 °C; Xu and Zhong, 2001). More importantly, the formation ages (ca. 299 Ma) of the STOB S-type granitoids are obviously earlier than that of the Tarim mantle plume, and thus do not support the plume model.

A post-collision setting for the late Carboniferous magmatic rocks in the STOB is also not supported. These rocks are mainly composed of calc-alkaline and intermediate-felsic rocks with minor amounts of mafic rocks (Jiang and others, 1999; Zhu and others, 2008a; Huang and others, 2012, 2015) and show enrichment in LILEs and depletion in HFSEs, more akin to typical island arc-type magmas. Meanwhile, the late

Carboniferous magmatic rocks in the western Tianshan show typical island arc geochemical characteristics, such as the Tekes gabbros (306 Ma; Zhu and others, 2011 and Qunjisayi rhyolites (306 Ma, Li and others, 2015). Other geological evidence also rules out a post-collision extensional setting including: (1) the eclogites in the Atbashi complex were formed at 224 to 217 Ma as recognized by Sang and others (2017), indicating that the South Tianshan ocean did not close until the Early Triassic; (2) late Permian turbidites are unconformably overlain by the Middle to Upper Triassic redbeds (Xiao and others, 2008), suggesting that final tectonic accretion took place between the latest Permian and the Triassic; (3) an early Permian (280 6 8 Ma) low-pressure, high-temperature metamorphic belt in Muzhaerte region of the STOB found by Gou and Zhang (2009), further indicative of a subduction zone. Therefore, combined with this study and previously published literature, the Tarim block did not collide with the Yili-Central Tianshan until the Permian.

Previous studies have shown that the Carboniferous magmatism in the STOB was mainly related to the northward subduction of the south Tianshan Ocean. Furthermore, the STOB has a Late Devonian to late Carboniferous (380–310 Ma) magmatic gap (figs. 15 and 16A). This magmatic quiescence period can be attributed to the flat-subduction of the south Tianshan oceanic slab (figs. 15 and 16A). Similar magmatic lulls also occurred in the Andes in response to flat slab subduction (Gutscher, 2002). Subsequently, the formation of a series of special rock associations (for example, bimodal volcanic rocks, A_2-type granitoids and granitic dikes) shows a late Carboniferous to Early Permian (310–285 Ma) magmatic "flare-up" in the CTS and STOB (fig. 15; Jiang and others, 2005; Long and others, 2008; Huang and others, 2012, 2013; Tang and others, 2014; Ma and others, 2015; Cheng and others, 2017; Tao and others, 2019). These characteristic rocks can serve as a powerful magmatic marker of a high temperature with extensional subduction setting. Furthermore, the temporal and spatial distributions of the magmatism suggest a southeastward migration as shown in figure 2. Therefore, we propose that the magmatism of this period is related to the slab roll-back of the south Tianshan ocean at this time (fig. 16B). In this slab roll-back model, asthenospheric mantle upwelling would have provided the heat source to cause the partial melting of lower crust and generated extensive magmatism and/or HT-LP metamorphism (Gutscher and others, 2000; Cawood and others, 2011; Tang and others, 2014; Yin and others, 2017).

Although sedimentary rocks may melt during steady state subduction (Guo and others, 2014), the complex succession of flat-slab subduction and subsequent slab roll-back may promote the recycling of sedimentary rocks (Hao and others, 2016). In this flat-slab subduction setting, large amounts of accretionary complex sediments could be easily subducted into the mantle by tectonic erosion, such as observed in the Andes-type subduction zone (von Huene and Scholl, 1991; Chapman and others, 2013). During flat-slab subduction, the cold wedge and lack of corner flow would have inhibited the melting of subduction sedimentary rocks (fig. 16A). Then, as the subduction angle increased, the asthenospheric mantle upwelling would drastically change the thermal state of the wedge and result in the partial melting of subducting sedimentary rocks to form the S-type granitoids in the STOB (fig. 16B). An analogous geodynamic process has been proposed in the circum-Pacific orogens (Collins and Richards, 2008) and western Kunlun, Northwest Tibet (Yin and others, 2020).

conclusions

1. The S-type granitoids in the STOB were emplaced in the late Carboniferous (ca. 299 Ma).

2. The S-type granitoids contain muscovite and have high $\delta^{18}O_{zrn}$ values indicating that they were derived from a metasedimentary rock source. However, the studied S-type granitoids show low A/CNK ratios (<1.1), and their P_2O_5 contents decrease with increasing SiO_2 contents, more typical of I-type granitoids. Therefore, using variation trends in P_2O_5 and A/CNK versus SiO_2 does not always provide a valid means to discriminate between I-type or S-type affinity of peraluminous granitoids.
3. Inherited zircon core ages and «Hf(t) values of the S-type granitoids are similar to those of the late Carboniferous metasedimentary rocks, but different from those of the Precambrian basement rocks, which further suggest that the S-type granitoids were derived from reworking of the late Carboniferous metasedimentary rocks in the STOB.
4. We propose that the late Carboniferous magmatism in the STOB was triggered by asthenospheric upwelling as a result of the slab rollback of the subducted south Tianshan ocean.

acknowledgments

We thank Guest Editors Professor Guochun Zhao and Simon Wilde and two anonymous reviewers for constructive reviews and comments that have greatly improved the quality of this paper.

This study was supported by the National Key R & D 445 Program of China (2017YFC0601206), National Science Foundation of China (Grant nos. 41888101, 41822204, 41830216 and 41873060), National Key Research and Development Project "Key scientific issues of transformative technology" (Grant no. 2019YFA0708601), the Fund from the Key Laboratory of Deep-Earth Dynamics of Ministry of Natural Resources (J1901-5), the China Geological Survey (Grant nos. DD20221649) and Hong Kong RGC grants (17303415 and 17302317). RS acknowledges funding under Natural Environment Research Council Grant NE/P017452/1 "From arc magmas to ores (FAMOS): A mineral systems approach". This is a contribution to the IGCP-662 project co-sponsored under the umbrella of IUGS and UNESCO.

references

Allen, M. B., Windley, B. F., and Chi, Z., 1993, Palaeozoic collisional tectonics and magmatism of the Chinese Tien Shan, central Asia: Tectonophysics, v. 220, n. 1–4, p. 89–115, https://doi.org/10.1016/0040-1951(93)90225-9

Altherr, R., and Siebel, W., 2002, I-type plutonism in a continental back-arc setting: Miocene granitoids and monzonites from the Central Aegean Sea, Greece: Contributions to Mineralogy and Petrology, v. 143, n. 4, p. 397–415, https://doi.org/10.1007/s00410-002-0352-y

Altherr, R., Holl, A., Hegner, E., Langer, C., and Kreuzer, H., 2000, High-potassium, calc-alkaline I-type plutonism in the European Variscides: northern Vosges (France) and northern Schwarzwald (Germany): Lithos, v. 50, n. 1–3, p. 51–73, https://doi.org/10.1016/S0024-4937(99)00052-3

Andersen, T., 2002, Correction of common lead in U-Pb analyses that do not report ^{204}Pb: Chemical Geology: Chemical Geology, v. 192, n. 1–2, p. 59–79, https://doi.org/10.1016/S0009-2541(02)00195-X

Appleby, S. K., Gillespie, M. R., Graham, C. M., Hinton, R. W., Oliver, G. J. H., and Kelly, N. M, EIMF., 2010, Do S-type granites commonly sample infracrustal sources?: Contributions to Mineralogy and Petrology, v. 160, n. 1, p. 115–132, https://doi.org/10.1007/s00410-009-0469-3

Belousova, E., Griffin, W., O'Reilly, S. Y., and Fisher, N., 2002, Igneous zircon: trace element composition as an indicator of source rock type: Contributions to Mineralogy and Petrology, v. 143, n. 5, p. 602–622, https://doi.org/10.1007/s00410-002-0364-7

Cawood, P. A., Leitch, E. C., Merle, R. E., and Nemchin, A. A., 2011, Orogenesis without collision: stabilizing the Terra Australis accretionary orogen, eastern Australia: Geological Society of America Bulletin, v. 123, n. 11–12, p. 2240–2255, https://doi.org/10.1130/B30415.1

Chapman, A. D., Saleeby, J. B., and Eiler, J., 2013, Slab flattening trigger for isotopic disturbance and magmatic flare-up in the southernmost Sierra Nevada batholith, California: Geology, v. 41, n. 9, p. 1007–1010, https://doi.org/10.1130/G34445.1

Chappell, B. W., 1999, Aluminium saturation in I- and S-type granites and the characterization of fractionated haplogranites: Lithos, v. 46, n. 3, p. 535–551, https://doi.org/10.1016/S0024-4937(98)00086-3

Chappell, B. W., and White, A. J. R., 1974, Two contrasting granite types: Pacific Geology: v, 8, p. 173–174.
Chappell, B. W., and White, A. J. R., 1992, I-Type and S-Type Granites in the Lachlan Fold Belt: Earth and Environmental Science Transactions of the Royal Society of Edinburgh v. 83, n. p. 1–2, p. 1, –26, https://doi.org/10.1017/S0263593300007720
Chappell, B. W., and White, A. J. R., 2001, Two contrasting granite types: 25 years later: Australian Journal of Earth Sciences, v. 48, n. 4, p. 489–499, https://doi.org/10.1046/j.1440-0952.2001.00882.x
Chappell, B. W., White, A. J. R., and Wyborn, D., 1987, The importance of residual source material (restite) in granite petrogenesis: Journal of Petrology, v. 28, n. 6, p. 1111–1138, https://doi.org/10.1093/petrology/28.6.1111
Chen, S. H., Zhong, W., and Zhang, J. R., 2019, Geochronology and geochemistry of the Jinghan granitic pluton in South Tianshan, Xinjiang and their tectonic significance: East China Geology, v. 41, p. 128–141 (in Chinese with English abstract).
Cheng, Z., Zhang, Z., Santosh, M., Zhao, Z., and Chen, L., 2017, Late Carboniferous to early Permian partial melting of the metasedimentary rocks and crustal reworking in the Central Asian Orogenic Belt: Evidence from garnet-bearing rhyolites in the Chinese South Tianshan: Lithos, v. 282–283, p. 373–387, https://doi.org/10.1016/j.lithos.2017.03.017
Clemens, J. D., and Stevens, G., 2012, What controls chemical variation in granitic magmas?: Lithos, v. 134–135, p. 317–329, https://doi.org/10.1016/j.lithos.2012.01.001
Collins, W. J., and Richards, S. W., 2008, Geodynamic significance of S-type granites in circum-Pacific orogens: Geology, v. 36, n. 7, p. 559–562, https://doi.org/10.1130/G24658A.1
Dan, W., Li, X. H., Wang, Q., Wang, X.-C., and Liu, Y., 2014, Neoproterozoic S-type granites in the Alxa Block, westernmost North China and tectonic implications: in situ zircon U-Pb-Hf-O isotopic and geochemical constraints: American Journal of Science, v. 314, n. 1, p. 110–153, 10.2475/01.2014.04
Dong, Y., Zhang, G., Neubauer, F., Liu, X., Hauzenberger, C., Zhou, D., and Li, W., 2011, Syn– and post–collisional granitoids in the Central Tianshan orogen: geochemistry, geochronology and implications for tectonic evolution: Gondwana Research, v. 20, n. 2–3, p. 568–581, https://doi.org/10.1016/j.gr.2011.01.013
Frost, B. R., Barnes, C. G., Collins, W. J., Arculus, R. J., Ellis, D. J., and Frost, C. D., 2001, A geochemical classification for granitic rocks: Journal of Petrology, v. 42, n. 11, p. 2033–2048, https://doi.org/10.1093/petrology/42.11.2033
Gao, J., Long, L., Klemd, R., Qian, Q., Liu, D., Xiong, X., Su, W., Liu, W., Wang, Y., and Yang, F., 2009, Tectonic evolution of the South Tianshan orogen and adjacent regions, NW China: geochemical and age constraints of granitoid rocks: International Journal of Earth Sciences, v. 98, n. 6, p. 1221–1238, https://doi.org/10.1007/s00531-008-0370-8
Gao, J., Klemd, R., Qian, Q., Zhang, X., Li, J., Jiang, T., and Yang, Y., 2011, The collision between the Yili and Tarim blocks of the Southwestern Altaids: geochemical and age constraints of a leucogranite dike crosscutting the HP–LT metamorphic belt in the Chinese Tianshan Orogen: Tectonophysics, v. 499, n. 1–4, p. 118–131, https://doi.org/10.1016/j.tecto.2011.01.001
Gao, P., Zhao, Z.-F., and Zheng, Y.-F., 2014, Petrogenesis of Triassic granites from the Nanling Range in South China: Implications for geochemical diversity in granites: Lithos, v. 210–211, p. 40–56, https://doi.org/10.1016/j.lithos.2014.09.027
Gao, P., Zheng, Y.-F., and Zhao, Z.-F., 2016, Distinction between S-type and peraluminous I-type granites: zircon versus whole-rock geochemistry: Lithos, v. 258–259, p. 77–91, https://doi.org/10.1016/j.lithos.2016.04.019
Gill, T. B., 1981, Orogenic Andesite and Plate Tectonics: Rocks & Minerals: Springer Science & Business Media, v. 16, p. 1–390, https://doi.org/10.1007/978-3-642-68012-0
Gou, L. L., and Zhang, L. F., 2009, Petrology and U–Th–Pb chemical monazite dating of the low-P metapelitic granulites at the region of Muzhaerte River in Southwestern Tianshan, NW China, and their geological implications: Acta Petrological Sinica, v. 25, p. 2271–2280 (in Chinese with English abstract).
Gou, L.-L., Zhang, L.-F., Lü, Z., and Shen, T.-T., 2015, Geochemistry and geochronology of S-type granites and their coeval MP/HT meta-sedimentary rocks in Chinese Southwest Tianshan and their tectonic implications: Journal of Asian Earth Sciences, v. 107, p. 151–171, https://doi.org/10.1016/j.jseaes.2015.04.020
Griffin, W. L., Wang, X., Jackson, S. E., Pearson, N. J., O'Reilly, S. Y., Xu, X., and Zhou, X., 2002, Zircon chemistry and magma mixing, SE China: In-situ analysis of Hf isotopes, Tonglu and Pingtan igneous complexes: Lithos, v. 61, n. 3–4, p. 237–269, https://doi.org/10.1016/S0024-4937(02)00082-8
Griffin, W. L., Pearson, N. J., Belousova, E. A., and Saeed, A., 2006, Comment: Hf-isotope heterogeneity in zircon 91500: Chemical Geology, v. 233, n. 3–4, p. 358–363, https://doi.org/10.1016/j.chemgeo.2006.03.007
Guo, Z. F., and Wilson, M., 2012, The Himalayan leucogranites: constraints on the nature of their crustal source region and geodynamic setting: Gondwana Research, v. 22, n. 2, p. 360–376, https://doi.org/10.1016/j.gr.2011.07.027
Guo, Z. F., Wilson, M., Zhang, L. H., Zhang, M. L., Cheng, Z. H., and Liu, J. Q., 2014, The role of subduction channel mélanges and convergent subduction systems in the petrogenesis of post-collisional K-rich mafic magmatism in NW Tibet: Lithos, v. 198, n. 1, p. 184–201, https://doi.org/10.1016/j.lithos.2014.03.020
Gutscher, M. A., 2002, Andean subduction styles and their effect on thermal structure and intraplate coupling: Earth and Planetary Science Letters: v. 15, p. 3–10, https://doi.org/10.1016/S0895-9811(02)00002-0
Gutscher, M. A., Maury, F., Eissen, J. P., and Bourdon, E., 2000, Can Slab Melting Be Caused by Flat Subduction?: Geology, v. 28, n. 6, p. 535–538, https://doi.org/10.1130/0091-7613(2000)28<535:CSMBCB.2.0.CO;2

Han, B.-F., He, G.-Q., Wang, X.-C., and Guo, Z.-J., 2011, Late Carboniferous collision between the Tarim and Kazakhstan–Yili terranes in the western segment of the South Tian Shan Orogen, Central Asia, and implications for the Northern Xinjiang, western China: Earth-Science Reviews, v. 109, n. 3–4, p. 74–93, https://doi.org/10.1016/j.earscirev.2011.09.001

Han, Y., and Zhao, G., 2018, Final amalgamation of the Tianshan and Junggar orogenic collage in the southwestern Central Asian Orogenic Belt: Constraints on the closure of the Paleo-Asian Ocean: Earth-Science Reviews, v. 186, p. 129–152, https://doi.org/10.1016/j.earscirev.2017.09.012

Han, Y., Zhao, G., Sun, M., Eizenhöfer, P. R., Hou, W., Zhang, X., Liu, Q., Wang, B., Liu, D., and Xu, B., 2016a, Late Paleozoic subduction and collision processes during the amalgamation of the Central Asian Orogenic Belt along the South Tianshan suture zone: Lithos, v. 246–247, p. 1–12, https://doi.org/10.1016/j.lithos.2015.12.016

Han, Y., Zhao, G., Cawood, P. A., Sun, M., Eizenhöfer, P. R., Hou, W., Zhang, X., and Liu, Q., 2016b, Tarim and North China cratons linked to northern Gondwana through switching accretionary tectonics and collisional orogenesis: Geology, v. 44, n. 2, p. 95–98, https://doi.org/10.1130/G37399.1

Han, Y., Zhao, G., Cawood, P. A., Sun, M., Liu, Q., and Yao, J., 2019, Plume-modified collision orogeny: The Tarim–western Tianshan example in Central Asia: Geology, v. 47, n. 10, p. 1001–1005, https://doi.org/10.1130/G46855.1

Hao, L.-L., Wang, Q., Wyman, D. A., Ou, Q., Dan, W., Jiang, Z.-Q., Yang, J.-H., Li, J., and Long, X.-P., 2016, Andesitic crustal growth via mélange partial melting: Evidence from Early Cretaceous arc dioritic/andesitic rocks in southern Qiangtang, central Tibet: Geochemistry: Geochemistry, Geophysics, Geosystems, v. 17, n. 5, p. 1641–1659, https://doi.org/10.1002/2016GC006248

Hopkinson, T. N., Harris, N. B. W., Warren, C. J., Spencer, C. J., Roberts, N. M. W., Horstwood, M. S. A., and Parrish, R. R., 2017, The identification and significance of pure sediment-derived granites: Earth and Planetary Science Letters, v, 467, p. 57–63, https://doi.org/10.1016/j.epsl.2017.03.018

Huang, H., Zhang, Z. C., Zhang, D. Y., Du, H. X., Ma, L. T., Kang, J. L., and Xue, C. J., 2011, Petrogenesis of Late Carboniferous to Early Permian Granitoid Plutons in the Chinese South Tianshan: implications for Crustal Accretion: Acta Geologica Sinica, v. 85, p. 1305–1333 (in Chinese with English abstract).

Huang, H., Zhang, Z. C., Kusky, T., Zhang, D. Y., Hou, T., Liu, J. L., and Zhao, Z. D., 2012, Geochronology and geochemistry of the Chuanwulu complex in the South Tianshan, western Xinjiang, NW China: Implications for petrogenesis and Phanerozoic continental growth: Lithos, v. 140–141, p. 66–85, https://doi.org/10.1016/j.lithos.2012.01.024

Huang, H., Zhang, Z. C., Santosh, M., Zhang, D. Y., Zhao, Z. D., and Liu, J. L., 2013, Early Paleozoic tectonic evolution of the South Tianshan Collisional Belt: evidence from geochemistry and zircon U–Pb geochronology of the Tie'reke Monzonite Pluton, Northwest China: The Journal of Geology, v. 121, n. 4, p. 401–424, https://doi.org/10.1086/670653

Huang, H., Zhang, Z. C., Santosh, M., Zhang, D. Y., and Wang, T., 2015, Petrogenesis of the Early Permian volcanic rocks in the Chinese South Tianshan: Implications for crustal growth in the Central Asian Orogenic Belt: Lithos, v. 228–229, p. 23–42, https://doi.org/10.1016/j.lithos.2015.04.017

Huang, H., Wang, T., Tong, Y., Qin, Q., Ma, X. X., and Yin, J. J., 2020, Rejuvenation of ancient micro-continents during accretionary orogenesis: Insights from the Yili Block and adjacent regions of the SW Central Asian Orogenic Belt: Earth-Science Reviews, https://doi.org/10.1016/j.earscirev.2020.103255

Jackson, S. E., Pearson, N. J., Griffin, W. L., and Belousova, E. A., 2004, The application of laser ablation-inductively coupled plasma-mass spectrometry to in situ U-Pb zircon geochronology: Chemical Geology, v. 211, n. 1–2, p. 47–69, https://doi.org/10.1016/j.chemgeo.2004.06.017

Jahn, B. M., Wu, F. Y., and Chen, B., 2000, Granitoids of the Central Asian Orogenic Belt and continental growth in the Phanerozoic: Earth and Environmental Science Transactions of the Royal Society of Edinburgh, v. 91, p. 181–193, https://doi.org//10.1130/0-8137-2350-7.181

Jeon, H., Williams, I. S., and Bennett, V. C., 2014, Uncoupled O and Hf isotopic systems in zircon from the contrasting granite suites of the New England Orogen, eastern Australia: implications for studies of Phanerozoic magma genesis: Geochimica et Cosmochimica Acta, v. 146, p. 132–149, https://doi.org/10.1016/j.gca.2014.09.042

Jiang, C. Y., Mu, Y. M., Bai, K. Y., Zhao, X. N., Zhang, H. B., and Hei, A. Z., 1999, Chronology, petrology, geochemistry and tectonic environment of granitoids in the southern Tianshan Mountain, western China: Acta Petrologica Sinica v 15, p. 298–308 (in Chinese with English Abstract).

Jiang, C. Y., Jiang, H. B., Ye, S. F., Xia, M. Z., and Lu, D. X., 2005, Petrochemical characteristics, Nd, Sr, Pb isotopic compositions and petrogenesis of Permian dike swarm, Kuruktag region , Xinjiang: Acta Geologica Sinica, v. 79, p. 823–833 (in Chinese with English abstract).

Kemp, A. I. S., Hawkesworth, C. J., Foster, G. L., Paterson, B. A., Woodhead, J. D., Hergt, J. M., Gray, C. M., and Whitehouse, M. J., 2007, Magmatic and Crustal Differentiation History of Granitic Rocks from Hf-O Isotopes in Zircon: Science, v. 315, n. 5814, p. 980–983, https://doi.org/10.1126/science.1136154

Kemp, A. I. S., Hawkesworth, C. J., Collins, W. J., Gray, C. M., and Blevin, P. L., 2009, Isotopic evidence for rapid continental growth in an extensional accretionary orogen: The Tasmanides, eastern Australia: Earth and Planetary Science Letters, v. 284, n. 3–4, p. 455–466, https://doi.org/10.1016/j.epsl.2009.05.011

Kong, W., Zhang, Z., Huang, H., Cheng, Z., and Santosh, M., 2019, Geochemistry and zircon U–Pb geochronology of the Oxidaban intrusive complex: Implication for Paleozoic tectonic evolution of the South Tianshan Orogenic Belt, China: Lithos, v. 324–325, p. 265–279, https://doi.org/10.1016/j.lithos.2018.11.013

Konopelko, D., Biske, G., Seltmann, R., Eklund, O., and Belyatsky, B., 2007, Hercynian post-collisional A-type granites of the Kokshaal Range, Southern Tien Shan, Kyrgyzstan: Lithos, v. 97, n.1–2, p. 140–160, https://doi.org/10.1016/j.lithos.2006.12.005

Konopelko, D., Seltmann, R., Biske, G., Lepekhina, E., and Sergeev, S., 2009, Possible source dichotomy of contemporaneous post-collisional barren I-type versus tin-bearing A-type granites, lying on opposite sides of the South Tien Shan suture: Ore Geology Reviews, v. 35, n. 2, p. 206–216, https://doi.org/10.1016/j.oregeorev.2009.01.002

Kröner, A., Hegner, E., Lehmann, B., Heinhorst, J., Wingate, M. T. D., Liu, D. Y., and Ermelov, P., 2008, Palaeozoic arc magmatism in the Central Asian Orogenic Belt of Kazakhstan: SHRIMP zircon ages and whole-rock Nd isotopic systematics: Journal of Asian Earth Sciences, v. 32, n. 2–4, p. 118–130, https://doi.org/10.1016/j.jseaes.2007.10.013

Li, J. Y., He, G. Q., Xu, X., Li, H. Q., Sun, G. H., Yang, T. N., Gao, L. M., and Zhu, Z. X., 2006, Crustal tectonic framework of northern Xinjiang and adjacent regions and its formation: Acta Geoscientica Sinica, v. 80, p. 148–168 (in Chinese with English Abstract).

Li, N.-B., Niu, H.-C., Shan, Q., and Yang, W.-B., 2015, Two episodes of Late Paleozoic A-type magmatism in the Qunjisayi area, western Tianshan: Petrogenesis and tectonic implications: Journal of Asian Earth Sciences, v. 113, p. 238–253, https://doi.org/10.1016/j.jseaes.2014.12.015

Li, Q.-L., Lin, W., Su, W., Li, X.-H., Shi, Y-h., Liu, Y., and Tang, G.-Q., 2011, SIMS U-Pb rutile age of low-temperature eclogites from southwestern Chinese Tianshan: NW China: Lithos, v. 122, n. 1–2, p. 76–86, https://doi.org/10.1016/j.lithos.2010.11.007

Li, S. Y., Yang, D. D., Wang, S., Wan, Q., and Wang, D. X., 2014, Characteristics of petrology, geochemistry, heavy minerals and isotope chronology of Upper Carboniferous detrital rocks in the middle segment of South Tianshan and constraints to the provenance and tectonic evolution: Acta Geologica Sinica, v. 88, p. 167–184 (in Chinese with English Abstract).

Li, X.-H., Li, W.-X., Li, Q.-L., Wang, X.-C., and Liu, Y.Y.Y.-H., 2010a, Petrogenesis and tectonic significance of the ; 850 Ma Gangbian alkaline complex in South China: Evidence from in situ zircon U–Pb dating: Hf–O Isotopes and Whole-Rock Geochemistry: Lithos, v. 114, n. 1–2, p. 1–15, https://doi.org/10.1016/j.lithos.2009.07.011

Li, X.-H., Long, W.-G., Li, Q.-L., Liu, Y., Zheng, Y.-F.Y.Y.-H., Chamberlain, K. R., Wan, D.-F., Guo, C.-H., Wang, X.-C., and Tao, H., 2010b, Penglai Zircon Megacrysts: a Potential New Working Reference Material for Microbeam Determination of Hf–O Isotopes and U–Pb Age: Geostandards and Geoanalytical Research, v. 34, n. 2, p. 117–134, https://doi.org/10.1111/j.1751-908X.2010.00036.x

Liang, Q., Jing, H., and Gregoire, D. C., 2000, Determination of trace elements in granites by inductively coupled plasma mass spectrometry: Talanta, v. 51, n. 3, p. 507–513, https://doi.org/10.1016/S0039-9140(99)00318-5

Liang, X. R., Wei, G. J., Li, X. H., and Liu, Y., 2002, Rapid and precise measurement for $^{143}Nd/^{144}Nd$ isotopic ratios using a multi-collector inductively coupled plasma mass spectrometer: Rock and Mineral Analysis, v. 21, p. 247–251(in Chinese with English Abstract).

Long, L., Jun, G., Wang, J., Qian, Q., Xiong, X., Wang, Y., Wang, L., and Gao, L., 2008, Geochemistry and SHRIMP Zircon U-Pb Age of Post-Collisional Granites in the Southwest Tianshan Orogenic Belt of China: Examples from the Heiyingshan and Laohutai Plutons: Acta Geologica Sinica - English Edition, v. 82, n. 2, p. 415–424, https://doi.org/10.1111/j.1755-6724.2008.tb00592.x

Long, L., Gao, J., Klemd, R., Beier, C., Qian, Q., Zhang, X., Wang, J., and Jiang, T., 2011, Geochemical and geochronological studies of granitoid rocks from the Western Tianshan Orogen: implications for continental growth in the southwestern Central Asian Orogenic Belt: Lithos: v. 126, n. 3–4, p. 321–340, https://doi.org/10.1016/j.lithos.2011.07.015

Ludwig, K. R., 2003, User's Manual for Isoplot 3.00: A Geochronological Toolkit for Microsoft Excel: Berkeley Geochronology Center, Special Publication, v. 4, p. 1–70.

Ma, L. T., Zhang, Z. C., Dong, S. Y., Zhang, S., Zhang, D. Y., and Huang, H., 2010, Geology and geochemistry of the Yingmailai granitic intrusion in the Southern Tianshan and its implications: Earth Science–Journal of China University of Geosciences, v. 35, p. 908–920 (in Chinese with English Abstract).

Ma, X., Shu, L., and Meert, J. G., 2015, Early Permian slab breakoff in the Chinese Tianshan belt inferred from the post-collisional granitoids: Gondwana Research: v. 27, n. 1, p. 228–243,https://doi.org/10.1016/j.gr.2013.09.018

Maniar, P. D., and Piccoli, P. M., 1989,Tectonic discrimination of granitoids: Geological Society of America Bulletin, v. 101, n. 5, p. 635–643, https://doi.org/10.1130/0016-7606(1989)101<0635:TDOG.2.3.CO;2

McCulloch, M. T., and Chappell, B. W., 1982, Nd isotopic characteristics of S- and I-type granites: Earth and Planetary Science Letters: v. 58, n. 1, p. 51–64, https://doi.org/10.1016/0012-821X(82)90102-9

Middlemost, E. A. K., 1994, Naming materials in the magma igneous rock system: Earth-Science Reviews, v. 37, n. 3–4, p. 215–224, 10.1016/0012-8252(94)90029-9

Reziwanguli, A., Zhu, Z. X., Jin, L. Y., Yang, S., Li, P., and Kahaer, N., 2019, Zircon U-Pb Age and Tectonic Implications of Quartz Diorite in the Southern Musitaosala Area, Central Tianshan Terrane, Xinjiang: Bulletin of Mineralogy, Petrology and Geochemistry, v. 38, p. 184–194 (in Chinese with English abstract).

Sang, M., Xiao, W., Bakirov, A., Orozbaev, R., Sakiev, K., and Zhou, K., 2017, Oblique wedge extrusion of UHP/HP complexes in the Late Triassic: structural analysis and zircon ages of the Atbashi Complex: South Tianshan, Kyrgyzstan: International Geology Review, v. 59, n, 10, p. 1369–1389, https://doi.org/10.1080/00206814.2016.1241163

Seltmann, R., Konopelko, D., Biske, G., Divaev, F., and Sergeev, S., 2011, Hercynian post-collisional magmatism in the context of Paleozoic magmatic evolution of the Tien Shan orogenic belt: Journal of Asian Earth Sciences, v. 42, n. 5, p. 821–838, https://doi.org/10.1016/j.jseaes.2010.08.016

Şengör, A. M. C., Natal'in, B. A., and Burtman, V. S., 1993, Evolution of the Altaid Tectonic Collage and Paleozoic Crustal Growth in Eurasia: Nature, v. 364, n. 6435, p. 299–307, https://doi.org/10.1038/364299a0

Stevens, G., Villaros, A., and Moyen, J.-F., 2007, Selective Peritectic Garnet Entrainment as the Origin of Geochemical Diversity in S-Type Granites: Geology, v. 35, n. 1, p. 9–12, https://doi.org/10.1130/G22959A.1

Su, W., Gao, J., Klemd, R., Li, J.-L., Zhang, X., Li, X.-H., Chen, N.-S., and Zhang, L., 2010, U–Pb zircon geochronology of Tianshan eclogites in NW China: implication for the collision between the Yili and Tarim blocks of the southwestern Altaids: European Journal of Mineralogy, v. 22, n. 4, p. 473–478, https://doi.org/10.1127/0935-1221/2010/0022-2040

Sun, S-S., and McDonough, W. F., 1989, Chemical and isotopic systematics of oceanic basalt: implications for mantle composition and processes , in Sanders, A. D., and Norry, M. J., editors, Magmatism in the Ocean Basins: Geological Society, London, Special Publications, v. 42, p. 313–345, https://doi.org/10.1144/GSL.SP.1989.042.01.19

Sylvester, P. J., 1998, Post-Collisional Strongly Peraluminous Granites: Lithos, v. 45, n. 1–4, p. 29–44, https://doi.org//10.1016/S0024-4937(98)00024-3

Tang, G.-J., Wang, Q., Wyman, D. A., Li, Z.-X., Xu, Y.-G., and Zhao, Z.-H., 2012, Metasomatized lithosphere–asthenosphere interaction during slab roll-back: evidence from Late Carboniferous gabbros in the Luotuogou area: Central Tianshan: Lithos, v. 155, p. 67–80, https://doi.org/10.1016/j.lithos.2012.08.015

Tang, G.-J., Chung, S.-L., Wang, Q., Wyman, D. A., Dan, W., Chen, H.-Y., and Zhao, Z.-H., 2014, Petrogenesis of a Late Carboniferous Mafic Dike–Granitoid Association in the Western Tianshan: Response to the Geodynamics of Oceanic Subduction: Lithos, v. 202–203, p. 85–99, https://doi.org/10.1016/j.lithos.2014.04.010

Tao, Z. L., Yin, J. Y., Chen, W., Li, D. P., Xu, Z. H., and Du, Q. U., 2019, Sr-Nd-Hf Isotopic Characteristics of Early Permian I-type Granites in the Southern Tianshan: Petrogenesis and Implication for Continental Crustal Growth: Earth Science, v. 44, p. 3565–3582 (in Chinese with English abstract).

Tian, W., Campbell, I. H., Allen, C. M., Guan, P., Pan, W., Chen, M., Yu, H., and Zhu, W., 2010, The Tarim Picrite–Basalt–Rhyolite Suite, a Permian Flood Basalt from Northwest China with Contrasting Rhyolites Produced by Fractional Crystallization and Anatexis: Contribution to Mineralogy and Petrology, v. 160, n. 3, p. 407–425, https://doi.org/10.1007/s00410-009-0485-3

Tian, Y. Z., Yang, J. S., Liu, F., Zhao, Y. J., Feng, G. Y., Niu, X. L., Zhang, L., and Gao, J., 2014, Petrological characteristics of Bulusitai gabbro and its constraint to the time of South Tianshan ocean subduction: Acta Petrologica Sinica, v. 30, p. 2363–2380 (in Chinese with English Abstract).

Valley, J. W., 2003, Oxygen Isotopes in Zircon: Reviews in Mineralogy and Geochemistry, v. 53, n. 1, p. 343–385, https://doi.org/10.2113/0530343

Valley, J. W., Kinny, P. D., Schulze, D. J., and Spicuzza, M. J., 1998, Zircon Megacrysts from Kimberlite: oxygen Isotope Variability among Mantle Melts: Contributions to Mineralogy and Petrology, v, 133, n. 1, p. 1–11, https://doi.org/10.1007/s004100050432

Valley, J. W., Lackey, J. S., Cavosie, A. J., Clechenko, C. C., Spicuzza, M. J., Basei, M., Bindeman, I. N., Ferreira, V. P., Sial, A. N., and King, E. M., 2005, 4.4 Billion Years of Crustal Maturation: Oxygen Isotope Ratios of Magmatic Zircon: Contributions to Mineralogy and Petrology, v, 150, n. 6, p. 561–580,https://doi.org/10.1007/s00410 -005 -0025 -8

Villaros, A., Stevens, G., Moyen, J.-F., and Buick, I. S., 2009, The Trace Element Compositions of S-Type Granites: evidence for Disequilibrium Melting and Accessory Phase Entrainment in the Source: Contributions to Mineralogy and Petrology, v. 158, n. 4, p. 543–561,, https://doi.org/10.1007/s00410-009-0396-3

Visona, D., and Lombardo, B., 2002, Two-mica and tourmaline leucogranites from the Everest-Makalu region (Nepal-Tibet): Himalayan Leucogranite Genesis by Isobaric Heating?: Lithos, v, 62, n. 3, p. 125–150, https://doi.org/10.1016/S0024-4937(02)00112-3

von Huene, R., and Scholl, D. W., 1991, Observations at convergent margins concerning sediment subduction, sediment erosion, and the growth of continental crust: Reviews of Geophysics: v. 29, n. 3, p. 279–316, https://doi.org/10.1029/91RG00969

Wang, B., Shu, L., Faure, M., Jahn, B.-M., Cluzel, D., Charvet, J., Chung, S.-L., and Meffre, S., 2011, Paleozoic tectonics of the southern Chinese Tianshan: Insights from structural: Chronological and Geochemical Studies of the Heiyingshan Ophiolitic Mélange (NW China): Tectonophysics, v, 497, p. n. 1–4, 85p. –104, https://doi.org/10.1016/j.tecto.2010.11.004

Wang, C., Liu, L., Che, Z. C., Luo, J. H., and Zhang, J. Y., 2007, Geochronology, petrogenesis and significance of Baleigong mafic rocks in Kokshal segment, southwestern Tianshan Mountains: Geological Review: v. 53, p. 743–753 (in Chinese with English abstract).

Wang, X.-S., Zhang, X., Gao, J., Li, J.-L., Jiang, T., and Xue, S.-C., 2018, A slab break-off model for the submarine volcanic-hosted iron mineralization in the Chinese Western Tianshan: Insights from Paleozoic subduction-related to post-collisional magmatism: Ore Geology Reviews, v. 92, p. 144–160, https://doi.org/10.1016/j.oregeorev.2017.11.015

Watson, E. B., and Harrison, T. M., 1983, Zircon Saturation Revisited: temperature and Composition Effects in a Variety of Crustal Magma Types: Earth and Planetary Science Letters, v, 64, n. 2, p. 295–304,https://doi.org/10.1016/0012-821X(83)90211-X

Wei, G.-J., Liang, X.-R., Li, X.-H., and Liu, Y., 2002, Precise measurement of Sr isotopic composition of liquid and solid base using (LP)MC-ICPMS: Geochimica, v. 31, p. 295–299 (in Chinese with English abstract).

Whalen, J. B., Currie, K. L., and Chappell, B. W., 1987, A-type granites: geochemical characteristics, discrimination and petrogenesis: Contributions to Mineralogy and Petrology, v. 95, n. 4, p. 407–419, https://doi.org/10.1007/BF00402202

White, A. J. R., and Chappell, B. W., 1977, Ultrametamorphism and granitoid genesis: Tectonophysics: v. 43n. 1–2, p. 7–22, https://doi.org/10.1016/0040-1951(77)90003-8

White, A. J. R., and Chappell, B. W.,, 1988, Some supracrustal (S-type) granites of the Lachlan Fold Belt: Earth and Environmental Science Transactions of the Royal Society of Edinburgh: v. 79, n. 2–3, p. 169–181, https://doi.org/10.1017/S026359330001419X

Windley, B. F., Alexeiev, D., Xiao, W. J., Kroner, A., and Badarch, G., 2007, Tectonic models for accretion of the Central Asian Orogenic Belt: Journal of the Geological Society, v. 164, p. 31–47, https://doi.org/10.1144/0016-76492006-022

Xiao, W. J., Han, C. M., Yuan, C., Sun, M., Lin, S. F., Chen, H. L., Li, Z. L., Li, J. L., and Sun, S., 2008, Middle Cambrian to Permian subduction–related accretionary orogenesis of North Xinjiang, NW China: implications for the tectonic evolution of Central Asia: Journal of Asian Earth Sciences, v. 32, n. 2–4, p. 102–117, https://doi.org/10.1016/j.jseaes.2007.10.008

Xiao, W. J., Kröner, A., and Windley, B. F., 2009, Geodynamic evolution of Central Asia in the Paleozoic and Mesozoic: International Journal of Earth Sciences, v. 98, n. 6, p. 1185–1188, https://doi.org/10.1007/s00531-009-0418-4

Xiao, W. J., Windley, B. F., Allen, M. B., and Han, C. M., 2013, Paleozoic Multiple Accretionary and Collisional Tectonics of the Chinese Tianshan Orogenic Collage: Gondwana Research, v. 23, n. 4, p. 1316–1341,, https://doi.org/10.1016/j.gr.2012.01.012

Xie, L. W., Zhang, Y. B., Zhang, H. H., Sun, J. F., and Wu, F. Y., 2008, situ simultaneous determination of trace elements: U-Pb and Lu-Hf Isotopes in Zircon and Baddeleyite: Chinese Science Bulletin, v. 53, n. 10, In p. 1565–1573, https://doi.org/10.1007/s11434-008-0086-y

Xu, X.-Y., Wang, H.-L., Li, P., Chen, J.-L., Ma, Z.-P., Zhu, T., Wang, N., and Dong, Y. -P., 2013, Geochemistry and geochronology of Paleozoic intrusions in the Nalati (Narati) area in western Tianshan, Xinjiang, China: implications for Paleozoic tectonic evolution: Journal of Asian Earth Sciences, v . 72, p. 33–62, https://doi.org/10.1016/j.jseaes.2012.11.023

Xu, Y. G., and Zhong, S. L., 2001, The Emeishan Large Igneous Province: Evidence for Mantle Plume Activity and Melting Conditions: Geochimica, v. 1: In Chinese with English Abstract), v. 1, p. 1–9,

Yang, L., Chen, W., Zhang, B., Yin, J. Y., Sun, J. B., Li, J., Yu, S., Yang, J., and Yuan, X., 2016, Ages and geochemistry of the Erbeng granite in southern Tianshan orogenic belt, Xinjiang: New constraints on the tectonic evolution of the southern Tianshan Ocean: Geological Bulletin of China v. 35, p. 152–166 (in Chinese with English Abstract)).

Yin, J. Y., Chen, W., Xiao, W. J., Zhang, B., Cai, K. D., Sun, J. B., Zhang, Y., Yang, J., Yang, L., Liu, X. Y., and Shen, Z., 2015, LA-ICP-MS zircon U-Pb age and geochemistry of the dark dykes in Central Tianshan Block: Geological Bulletin of China, v. 34, p. 1470–1481 (in Chinese with English Abstract).

Yin, J., Chen, W., Xiao, W., Yuan, C., Zhang, B., Cai, K., and Long, X., 2017, Geochronology, petrogenesis, and tectonic significance of the latest Devonian–early Carboniferous I-type granites in the Central Tianshan: NW China: Gondwana Research, v, 47, p. 188–199, https://doi.org/10.1016/j.gr.2016.02.012

Yin, J., Xiao, W., Sun, M., Chen, W., Yuan, C., Zhang, Y., Wang, T., Du, Q., Wang, X., and Xia, X., 2020, Petrogenesis of Early Cambrian granitoids in the western Kunlun orogenic belt , Northwest Tibet: Insight into early stage subduction of the Proto-Tethys Ocean: Geological Society of America Bulletin, v. 132, n. 9–10, p. 2221–2240, https://doi.org/10.1130/B35408.1

Yu, S., Zhang, J., Li, S., Santosh, M., Li, Y., Liu, Y., Li, X., Peng, Y., Sun, D., Wang, Z., and Lv, P., 2019a, TTG-Adakitic-Like (Tonalitic-Trondhjemitic) Magmas Resulting From Partial Melting of Metagabbro Under High-Pressure Condition During Continental Collision in the North Qaidam UHP Terrane, Western China: Tectonics, v. 38, n. 3, p. 791–822, https://doi.org/10.1029/2018TC005259

Yu, S., Li, S., Zhang, J., Peng, Y., Somerville, I., Liu, Y., Wang, Z., Li, Z., Yao, Y., and Li, Y., 2019b, Multistage anatexis during tectonic evolution from oceanic subduction to continental collision: A review of the North Qaidam UHP Belt, NW China: Earth-Science Reviews, v. 191, p. 190–211, https://doi.org/10.1016/j.earscirev.2019.02.016

Yuan, C., Sun, M., Wilde, S., Xiao, W., Xu, Y., Long, X., and Zhao, G., 2010, Post–collisional plutons in the Balikun area, East Chinese Tianshan: evolving magmatism in response to extension and slab break-off: Lithos, v. 119, n. 3–4, p. 269–288, https://doi.org/10.1016/j.lithos.2010.07.004

Zen, E.-A., 1986, Aluminum enrichment in silicate melts by fractional crystallization: some mineralogic and petrographic constraints: Journal of Petrology, v. 27, n. 5, p. 1095–1117, https://doi.org/10.1093/petrology/27.5.1095

Zhang, C.-L., and Zou, H.-B., 2013, Permian A-type granites in Tarim and western part of Central Asian Orogenic Belt (CAOB): genetically related to a common Permian mantle plume?: Lithos, v. 172–173, p. 47–60, https://doi.org/10.1016/j.lithos.2013.04.001

Zhang, C.-L., Li, X.-H., Li, Z.-X., Ye, H.-M., and Li, C.-N., 2008, A Permian layered intrusive complex in the western Tarim Block, northwestern China: product of a Ca. 275-Ma mantle plume?: Journal of Geology, v. 116, n. 3, p. 269–287,https://doi.org/10.1086/587726

Zhang, H., Harris, N., Parrish, R., Kelley, S., Zhang, L., Rogers, N., Argles, T., and King, J., 2004, Causes and consequences of protracted melting of the mid-crust exposed in the North Himalayan antiform: Earth and Planetary Science Letters: v. 228, n. 1–2, p. 195–212, https://doi.org/10.1016/j.epsl.2004.09.031

Zhang, L., Ai, Y., Li, X., Rubatto, D., Song, B., Williams, S., Song, S., Ellis, D., and Liou, J. G., 2007, Triassic collision of western Tianshan orogenic belt: China: Evidence from SHRIMP U–Pb Dating of Zircon from HP/UHP Eclogitic Rocks: Lithos, v. 96, n. 1–2, p. 266–280, https://doi.org/10.1016/j.lithos.2006.09.012

Zhao, Z.-F., Gao, P., and Zheng, Y.-F., 2015, The source of Mesozoic granitoids in South China: Integrated geochemical constraints from the Taoshan batholith in the Nanling Range: Chemical Geology: v, 395, p. 11–26, https://doi.org/10.1016/j.chemgeo.2014.11.028

Zhu, D. C., Mo, X. X., Niu, Y. L., Zhao, Z. D., Wang, L. Q., Pan, G. T., and Wu, F. Y., 2009, Zircon U-Pb dating and in-situ Hf isotopic analysis of Permian peraluminous granite in the Lhasa terrane, southern

Tibet: Implications for Permian collisional orogeny and paleogeography: Tectonophysics: v. 469, n. 1–4, p. 48–60, https://doi.org/10.1016/j.tecto.2009.01.017

Zhu, M. T., Wu, G., Xie, H. J., Liu, J., and Zhang, L. C., 2011, Geochronology and geochemistry of the Kekesai intrusion in western Tianshan, NW China and its geological implications: Acta Petrologica Sinica, v. 10, p. 3041–3054 (in Chinese with English abstract).

Zhu, Z. X., Li, J. Y., Dong, L. H., Zhang, X. F., Hu, J. W., and Wang, K. Z., 2008a, The age determination of Late Carboniferous intrusions in Mangqisu region and its constraints to the closure of oceanic basin in South Tianshan, Xinjiang: Acta Petrologica Sinica, v, 2412, p. 2761–2766,in Chinese with English abstract).

Zhu, Z. X., Li, J. Y., Dong, L. H., Wang, K. Z., Liu, G. Z., Li, Y. P., and Liu, Z. H., 2008b, Age determination and geological significance of Devonian granitic intrusion in Serikeyayilake region, northern margin of Tarim basin: Acta Petrologica Sinica, v 24, p. 971–976 (in Chinese with English abstract).